



DISSERTATION DEVELOPED IN THE AMBIT OF THE INTEGRATED MASTER IN BIOENGINEERING SPECIALIZATION IN MOLECULAR BIOTECHNOLOGY

VERTEPORFIN-LOADED LIPID NANOPARTICLES FOR PHOTODYNAMIC THERAPY OF CANCER

Tomás Duarte Mendes

Supervisor: Prof. Dr. Salette Reis Laboratory tutor: MSc Andreia Granja

September 15th 2022

Acknowledgement

To all the people who were there and could see me grow both personally and professionally, I want to thank them for making this possible.

First of all, to my advisor Salette Reis and lab tutor Andreia Granja with whom I had the pleasure of working and learning throughout this year. To Salette for accepting me and for all the trust in such an interesting and unique project and to Andreia for her wealth of knowledge and valuable feedback, help with the manuscript, and for always providing advice that I value greatly. I am very grateful to you both.

I want to thank to all my lab fellows for the knowledge they transmitted to me, for their patience, for all the help, kindness and encouragement.

To my friends, to whom I have nothing but immense gratitude for their support, and for always helping me stay on track. In particular to my girlfriend for her patience, care, and unconditional support during all these years of university.

Lastly, I thank from the bottom of my heart to my incredible family. Pai, Mãe, Irmão, your unconditional love makes everything possible.

Abstract

Cancer is one of the major causes of illness and mortality around the world. The traditional chemotherapy regimens used to treat this disease frequently result in severe side-effects and poor efficacy. Drug delivery systems have opened up new possibilities for enhancing the therapeutic benefits and limiting the systemic side-effects of chemotherapeutic drugs. Solid Lipid Nanoparticles have emerged as particularly promising nanocarriers in cancer treatment. Low toxicity, high drug bioavailability, adaptability in incorporating hydrophilic and lipophilic medicines, and large-scale production feasibility are all advantages of this type of nanoparticles.

In this work SLN loaded with the photosensitizer Verteporfin (VP) were produced to increase VP bioavailability and active cancer cell targeting through functionalization with Folic acid. The purpose of this formulation is to be intravenous administrated and the subsequent use of Photodynamic therapy as the method to activate VP, produce Reactive Oxygen Species and induce cancer cell death.

The produced nanoparticles were characterized in terms of mean particle size, polydispersity index, zeta potential and encapsulation efficiency. The particle size obtained varied between 193 ± 8 nm to 225 ± 3 nm, which is an adequate size for intravenous administration. A highly negative zeta potential (around -25mV) was obtained, which indicates a good nanoparticle physical stability. Moreover, the encapsulation efficiency of VP range above 95%, over 3 months of the stability study.

The *in vitro* studies support that VP-loaded nanoparticles are safe and efficient for intravenous administration, as observed by absence of hemolytic activity and toxicity to the reference cell line L929. The photodynamic therapeutic effect of the nanoformulations was then studied. To do so, an optimization process was carried out where different light irradiation doses, exposure times and concentrations of VP were studied. After establishing the optimum conditions, it was demonstrated that VP-loaded SLN photodynamic therapeutic effect was successful against the human breast cancer cell line MCF-7, while having very low dark toxicity at the same of range of concentrations. Comparing to the free VP, the encapsulation of VP possibly resulted in a more controlled drug release, leading to less immediate anti-cancer effects than the free drug. Nevertheless, it was demonstrated that the developed nanoformulation still showed a high anti-cancer activity upon light irradiation. This was also reflected into an enhanced production of Reactive oxygen species and induction of cancer cell apoptosis.

In conclusion, the results obtained supported the idea that VP is a very efficient anticancer photosensitizer and suggested that VP-functionalized loaded NPs may show interesting therapeutic potential for management of cancer disease.

Table of contents

1	Cha	pter Introduction	1
	1.1	Cancer disease	1
	1.2	Photodynamic therapy	2
	1.3	Photosensitizers	9
	1.4	Nanotechnology role in Photodynamic therapy	16
	1.5	Aims and objectives	21
2	Cha	pter Materials and Methods	22
	2.1	Materials	22
	2.2	Production of Solid Lipid Nanoparticles	22
	2.3 (DSPF-F	Synthesis of Disteroylphosphatidylethanolamine-poly (ethylene glycol)2000-folic PEG2000-FA) Conjugate	
	2.4	Production of Functionalized Solid Lipid Nanoparticles	
	2.5	Nanoparticle Characterization	
	2.6	Cellular studies	27
3	Cha	pter Results and Discussion	33
	3.1	Production of Verteporfin-loaded solid lipid nanoparticles	33
	3.2	Physicochemical characterization	33
	3.3	Stability studies	34
	3.4	Cellular studies	35
	3.5	In vitro photodynamic therapy studies	38
4	Cha	pter Conclusion and Future Prospects	44

List of figures FIGURE 1 - TYPE I AND TYPE II

FIGURE 1 - TYPE I AND TYPE II REACTIONS IN PDT. SCHEMATIC DIAGRAM SHOWING PDT'S MECHANISM OF ACTION3
FIGURE 2 - THE THREE MOST NOTED PATHWAYS OF CELL DEATH
FIGURE 3 - CHEMICAL STRUCTURE OF VERTEPORFIN
FIGURE 4 - SCHEMATIC REPRESENT OF LIPID NANOPARTICLES, INCLUDING SLN AND NLC
FIGURE 5 - SCHEMATIC REPRESENTATION OF ZETA POTENTIAL (Z)
FIGURE 6- EFFECT OF TIME OF STORAGE ON (A) SIZE. (B) PDI OF THE NANOFORMULATIONS. (C) EFFECT OF
TIME OF STORAGE ON ZETA POTENTIAL OF VP-LOADED NANOFORMULATIONS FUNCTIONALIZED AND
NONFUNCTIONALIZED WITH DSPE.PEG-FA CONJUGATE. (D) EFFECT OF TIME OF STORAGE ON EE OF VP-
LOADED NANOFORMULATIONS FUNCTIONALIZED AND NONFUNCTIONALIZED WITH DSPE.PEG-FA
CONJUGATE. VALUES REPRESENT THE MEAN ± SD (N=3), *P<0.05, **P<0.01. ALL STATISTICALLY
SIGNIFICANT DIFFERENCES ARE RELATED TO THE VALUES OF THE CORRESPONDENT NANOPARTICLES AT
WEEK O. DIFFERENCES BETWEEN GROUPS WERE DETERMINED USING TWO-WAY ANOVA FOLLOWED BY
DUNNETT'S MULTIPLE COMPARATIONS TEST
Figure 7 - (A) In vitro hemolysis assay results for diluted human blood exposed to different
CONCENTRATIONS (2, 4, 8, 16, 32 (MM) OF FREE VP AND VP-LOADED FORMULATIONS. (B) IS AN
Amplified view of (A). Values represent mean \pm SD (N=3)), (*) denotes statistically
SIGNIFICANT DIFFERENCES RELATIVELY TO THE CORRESPONDENT FREE VP 16 MM (P<0.05).
DIFFERENCES BETWEEN GROUPS WERE DETERMINED USING TWO-WAY ANOVA FOLLOWED BY TUKEY'S
MULTIPLE COMPARATIONS TEST
FIGURE 8 - CLSM IMAGES OF THE MCF-7 CELLULAR UPTAKE OF VP LOADED SLN, FREE VP AND CONTROL.
Cells were incubated with the nanoformulations for 3 h. Blue channel: Hoechst 33342
(NUCLEUS). RED CHANNEL: VP
Figure 9 - Dose-response curves of MCF-7 cells incubation with free VP for 24h
FIGURE 10 - MCF-7 CELL VIABILITY ASSESSED BY THE RESAZURIN ASSAY AFTER 24 H OF EXPOSURE TO THE
DIFFERENT NANOFORMULATIONS AND FREE VP AT INCREASING CONCENTRATIONS OF SLN,
REPRESENTING THE DARK TOXICITY OF THE NANOFORMULATIONS AND FREE VP. VALUES REPRESENT THE
MEAN \pm SD (N>3)
FIGURE 11 - MCF-7 CELL VIABILITY ASSESSED BY RESAZURIN ASSAY AFTER 24 H OF EXPOSURE TO THE
DIFFERENT TIMES (A) AND DIFFERENT INTENSITIES (B), NOT EXPOSED TO LIGHT. VALUES REPRESENT THE
MEAN \pm SD (N>3) (****) DENOTES STATISTICALLY SIGNIFICANT DIFFERENCES OF P<0.0001 RELATIVELY
TO THE CORRESPONDENT CONTROL. DIFFERENCES BETWEEN GROUPS WERE DETERMINED USING TWO-
WAY ANOVA FOLLOWED BY DUNNETT'S MULTIPLE COMPARATIONS TEST
FIGURE 12 - MCF-7 CELL VIABILITY ASSESSED BY RESAZURIN ASSAY AFTER 24 H OF EXPOSURE TO THE
DIFFERENT NANOFORMULATIONS AND FREE VP AT INCREASING CONCENTRATIONS OF SLN, EXPOSED TO
LIGHT (PDT TREATMENT). VALUES REPRESENT THE MEAN ± SD (N>3). *P<0.05, **P<0.01,

0001 DENOTES STATISTICALLY SIGNIFICANT DIFFERENCES. DIFFERENCES BETWEEN GROUPS					
TERMINED USING TWO-WAY ANOVA FOLLOWED BY TUKEY 'S MULTIPLE COMPARATIONS TEST. 41					
APOPTOSIS OF MCF-7 CELLS FOLLOWING INCUBATION WITH THE NANOFORMULATIONS AT A	FIGURE 13				
ration of $0.125\mu\text{M}$ of VP using the FITC Annexin V Apoptosis assay. Data expressed					
\pm SD (N = 2) ALL STATISTICALLY SIGNIFICANT DIFFERENCES ARE THE DIFFERENCES BETWEEN					
ATMENT AND CONTROL GROUP: VIABLE: **** P < 0.0001; EARLY APOPTOSIS: ++++ P < 0.0001					
ICES BETWEEN GROUPS WERE DETERMINED USING TWO-WAY ANOVA FOLLOWED BY DUNNETT'S					
COMPARATIONS TEST42					
QUANTIFICATION OF MCF-7 CELLULAR UPTAKE OF VP-LOADED SLN AND FREE VP BY FLOW	Figi				
RY. CELLS WERE INCUBATED FOR 3H WITH AN EQUIVALENT CONCENTRATION OF $0.25\mu\text{M}$ of VP					
LIGHT AND LIGHT. DATA EXPRESSED AS MEAN \pm SD (N=2)43					

List of Tables

TABLE 1 - ADVANTAGES AND DISADVANTAGES OF PDT IN CANCER	.9
TABLE 2 - PHYSICOCHEMICAL CHARACTERIZATION OF THE FINAL FORMULATIONS: SIZE, PDI, ZETA POTENTIA	L
EE AND LC.	34

List of equations

EQUATION 1	25
EQUATION 2	27
EQUATION 3	27
EQUATION 4	28
EQUATION 5	29
EQUATION 6	31
EQUATION 7	31

Abbreviations

AMD Age-related macular degeneration

7-AAD 7-amino-actinomycin D APCs Antigen-presenting cells

CLSM Confocal laser scanning microscopy

DAMPs Damage associated molecular patterns

DCC Dicyclohexylcarbodiimide DCF 2',7'-dichlorofluorescin

DCFDA 2',7'-Dichlorofluorescein diacetate

DCs Dendritic cells
DCU Dicylcohexylurea

DLS Dynamic light scattering

DMEM Dulbecco's Modified Eagle's Medium

DMSO Dimethyl sulfoxide
DNA Deoxyribonucleic acid

Disteroylphosphatidylethanolamine-poly(ethylene glycol)-Folic

DSPE-PEG-FA acid

EE Encapsulation efficiency

EGFR Epidermal growth factor receptors
ELS Electrophoretic light scattering

FA Folic Acid

FBS Fetal Bovine Serum

FITC Fluorescently labeled with Fluorescein isothiocyanate

FR Folate receptors

GRAS Generally recognized as safe

H2O2 Hydrogen peroxide HO• Hydroxyl radical

HPD Hematoporphyrin derivative HPH High-pressure homogenization

LC Loading capacity

MCF-7 Michigan Cancer Foundation-7

NHS N-Hydroxysuccinimide

NK Natural killer
NPs Nanoparticles

NTA Nanoparticle tracking analysis

O2•- Superoxide anion

OH- Hydroxide ion
ONOO- Peroxynitrite

PBS Phosphate Buffered Saline

PDI Polydispersity Index
PDT Photodynamic therapy

PS Photosensitizer
RBC Red blood cells

RFU Relative fluorescence units
ROS Reactive Oxygen Species
SLN Solid Lipid Nanoparticles
SOD Superoxide dismutase

TEA Triethylamine

TfR Transferrin-receptors
TNFs Tumor necrosis factors

VEGF Vascular endothelial growth factor

VP Verteporfin

1 Chapter Introduction

1.1 Cancer disease

Cancer is characterized by an uncontrolled division and growth of abnormal cells. This is caused by several gene expression alterations, which affect the normal mechanisms of cell division and differentiation. Different factors that can induce genetic mutations and, consequently, cancer development, such as unhealthy diet, tobacco and radiation, as external factors and inherited genetic mutations and immune conditions as internal factors [1, 2].

This disease is one of the main causes of morbidity and mortality globally. In 2020, approximately 19.3 million new cases were diagnosed and almost 10 million cancer-related deaths occurred worldwide [3]. The economic impact of cancer is also factor that should be taken into account. In 2020, the total healthcare expenses associated with cancer in the US were \$208.9 billion [4]. Across the Europe, the health-care costs of cancer were to €126 billion in 2009 [5].

Nowadays cancer treatments are mainly based on the removal of the tumor by either surgery or radiotherapy and often combined with systemic adjuvant therapies such as chemotherapy and hormonal therapies [6]. Nevertheless, there are various adverse effects of regularly prescribed chemotherapy drugs such as tiredness, anemia, weight loss and vomiting, reduced quality of life and, eventual death due to limited treatment efficacy and recurrence of the disease [6-8]. Therefore, the main problem with the use of conventional medicines to treat cancer patients is that these therapies typically have a low selectivity to cancer cells, which leads to systemic distribution and toxicity [9]. Patients who receive these types of treatment frequently experience significant unintended side-effects due to the large toxic drug loads' tendency to additionally harm normal body cells. Additionally, tumor heterogeneity and medication resistance present significant challenges for the majority of traditional cancer treatments [10].

In this aspect, nanoparticles (NPs) have emerged as a new opportunity in cancer therapy, since they are able to improve the selectivity towards their target, display a controlled release of their load, improve the drug pharmacokinetics by enhancing its aqueous solubility, half-life time in blood and permeability across different biological barriers, and decrease the off-target distribution and systemic toxicity, by improving the accumulation of the drug at the tumor site [11, 12].

1.2 Photodynamic therapy

1.2.1 History of photodynamic therapy

For thousands of years, light has been one of the elements used in the treatment of various diseases. By combining psoralenes and sunshine, the Egyptians, Indians, and Chinese employed light to heal skin conditions like psoriasis, vitiligo, and cancer [13]. The Danish physician Niels Finsen introduced phototherapy at the end of the 19th century after learning that smallpox could be treated by exposing patients to red light, which prevented the development of pustules [14]. In addition to this discovery, Niels Finsen used UV light from the sun to treat tuberculosis of the skin and was awarded the Nobel Prize in 1903 [13].

Early in the 20th century, Oscar Raab observed that the presence of radiation and a few specific substances induced cell death while collaborating with Professor Herman von Tappeiner. The neurologist Jean Prime discovered that epileptic patients receiving oral eosin developed dermatitis in areas exposed to sunshine at the same time. This gave rise to the first use of eosin and white light in medicine for the treatment of skin cancers. Later, in 1907, Herman von Tappeiner and Albert Joldbauer showed that oxygen is required for photosensitizing reactions to occur, and they coined the name "photodynamic action" to describe this phenomenon [13, 15].

Photodynamic therapy development stalled for years, and it was not until the mid-1960s that the introduction of a hematoporphyrin derivative (HPD) reignited interest in this therapy. Lipson and Baldes used animals to show that HPD applied at low dosages was more efficient than hematoporphyrin at localizing and differentiating tumor cells [13]. When Dougherty and his associates used red-light activated HPD to completely eradicate malignant breast cancers in mice and then in humans with tumors of the breast, colon, skin, and prostate, it marked one of the key turning points in the development of PDT [13, 15]. Despite this latter achievement, Photofrin®, the first photosensitizer (PS) for the treatment of bladder cancer, was not licensed in Canada until the early 1990s [14]. Later, it received permission in several nations for the treatment of additional tumors, including bronchial cancer, esophageal cancer, and Barret's esophagus. Although this first-generation PS has proven effective against a number of cancer types, it has numerous limitations, including poor tumor selectivity, weak light penetration, and skin photosensitivity. Numerous second-generation PS were developed in order to increase efficacy and reduce side-effects, including temoporphine (Foscan®) and verteporfin (Visudyne®), which are recommended for the treatment of head and neck cancer and age-related macular degeneration (AMD), respectively [16, 17].

More recently, researchers have been working on the development of third-generation PS, which can be activated by higher wavelength light, be more selective to tumor tissues, and in which photosensitivity in patients is reduced or eliminated. A third-generation PS with orphan drug status for the treatment of cholangiocarcinoma, a serious tumor of the biliary tract, is redaporfin, which is now in clinical phase I/II [18].

1.2.2 Mechanism of action

The main objective of PDT is to selectively destroy the target tissue while causing the least amount of collateral damage to the nearby healthy tissues. For this effect to occur, the simultaneous existence in the target tissue of three essential components is required: visible light, molecular oxygen and the PS (Figure 1) [17].

After the PS has been administered and has accumulated in the target tissue, a photodynamic response caused by irradiation and subsequent light absorption by the PS takes place. This results in a sequence of photochemical reactions that produce reactive oxygen species (ROS), which harm the target tissue [14].

PS in the fundamental state has two electrons with opposite spin orientation (singlet fundamental state). After light absorption, the PS is excited (singlet excited state). After excitation, the PS can return to the fundamental state with fluorescence or heat emission or undergo the intersystem crossing phenomenon. The return to the fundamental state through emission of radiation by fluorescence or heat may allow development of techniques for determining the concentration of PS in tissues. The intersystem crossing over phenomenon consists in the spin inversion of an electron in the excited state originating the triplet excited state with a longer lifetime than the singlet excited state. It is in this state that the PS will interact with molecular oxygen and initiate the ROS formation process [17].

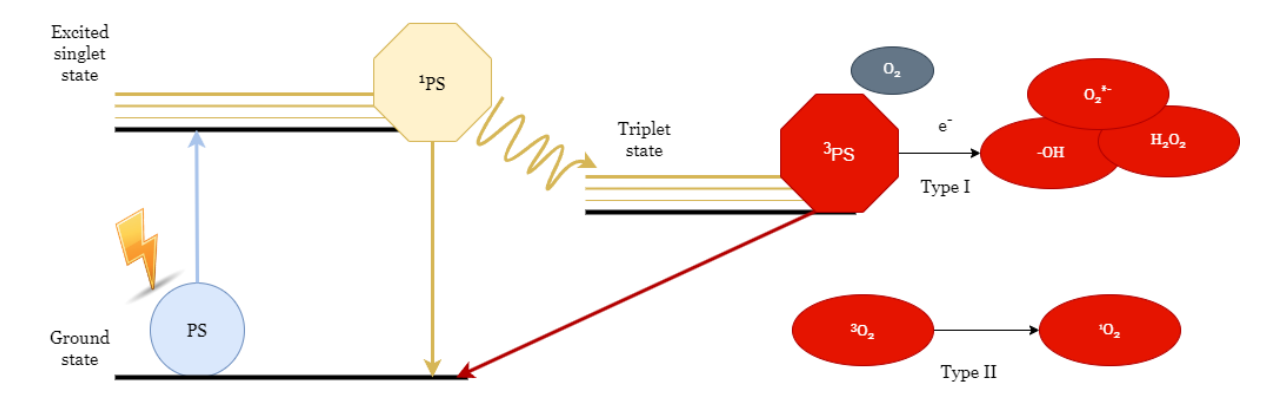


Figure 1 - Type I and Type II reactions in PDT. Schematic diagram showing PDT's mechanism of action.

The formation of ROS can occur through two types of reactions:

Type I - Direct reaction with O_2 or with an organic molecule giving rise to the formation of superoxide anion ($O_2^{\bullet-}$) or transfer of a proton or electron, giving rise to an anion or proton radical.

Type II - energy transfer to the O_2 in the fundamental state (triplet) forming the excited O_2 (singlet oxygen, ${}^{1}O_2$) [17].

The type I reaction initially forms O_2^{\bullet} , which is less reactive and does not cause significant oxidative damage. However, it can give rise to hydrogen peroxide (H_2O_2) through the dismutation reaction that is catalysed by the enzyme superoxide dismutase (SOD). In addition to dismutation, O_2^{\bullet} is important in starting the chain of ROS formation by reducing metal ions (such as Fe^{3+}) that catalyse the conversion of H_2O_2 by breaking oxygen bonds into hydroxide ion (OH-) and hydroxyl radical (HO $^{\bullet}$) - Fenton reaction. Superoxide can also react with the hydroxyl radical forming singlet oxygen or with nitric oxide producing another very reactive species, such as peroxynitrite (ONOO-) [17].

In the type II reaction, the mechanism is very simple with a direct transfer of energy to the O_2 molecule, leading to the formation the reactive species ${}^{1}O_2$. This reaction tends to occur more often than the type I reaction due to its simpler mechanism and the fact that it is thermodynamically favored, which makes ${}^{1}O_2$ the major mediator in PDT [19].

The ROS formed by these reactions affect many biomolecules (deoxyribonucleic acid (DNA), lipids or proteins) near the area of origin due to their high reactivity and low half-life time, as is the case of ${}^{1}O_{2}$ and HO•. Examples of biomolecules that undergo oxidation are protein residues of amino acids such as tyrosine, tryptophan, methionine, cysteine, and histidine, unsaturated lipids from cell membranes and other organelles, and nucleotides, notably guanine, causing DNA disruption and inducing cell death [20].

Type I and type II reactions can occur simultaneously, leading to an amplified response to therapy. However, the extent of the type I or II mechanism will be defined by the type of PS, the presence of oxygen, the affinity of the PS for the target tissue, and the amount at the target tissue. The damage caused also depends on the amount of oxygen and the type of PS, in addition to other factors, such as the total dose administered, the time of light exposure and the time between administration and light exposure (drug light interval), all of which are interdependent [14].

1.2.3 Tumor Destruction

Being the main aim of PDT the eradication of the tumor, three mechanisms of tumor destruction have been identified that play a key role in achieving this goal. These mechanisms

are interconnected and consist of a direct effect on tumor cells, a vascular effect or an effect on the immune system Figure 2 [21].

The direct effect on tumor cells can occur via apoptosis, necrosis, and autophagy, which are three different ways of cell death that are brought on by the irreversible oxidative damage that ROS cause to biomolecules and cellular structures (Figure 2). The mode and extent of cell death are influenced by the physicochemical properties, concentration and location of PS, as well as by the oxygen concentration and the intensity and wavelength of the radiation source used [22].

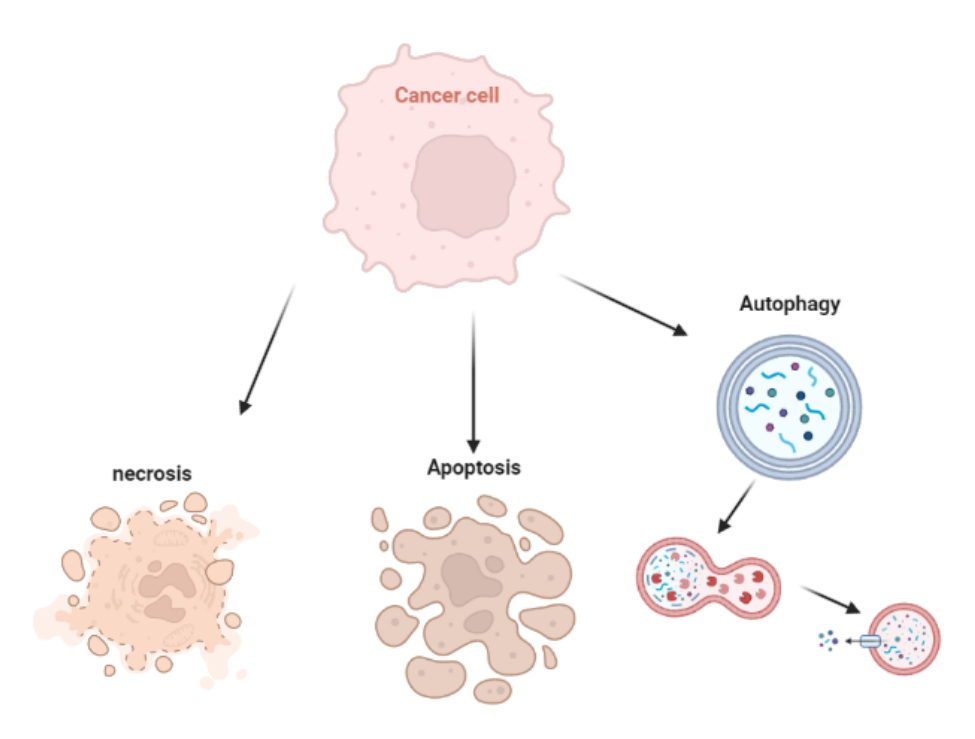


Figure 2 - The three most noted pathways of cell death.

1.2.3.1 Apoptosis

Apoptosis is a programmed, energy-dependent mechanism of cell death characterized by nuclear condensation, cleavage of chromosomal DNA, cell contraction, formation of apoptotic bodies, and exposure to phosphatidylserine on the outer side of the cell membrane. This mechanism involves the activation of caspases, responsible for most of the alterations described, which act through an extrinsic and an intrinsic pathway [23].

In the extrinsic pathway, the binding of apoptosis inducers (such as Tumor Necrosis Factor-alpha, TNF- α) to their receptors occurs. After this binding, formation of the death-inducing signaling complex occurs that will initiate the activation of the initiator procaspase-8. Subsequently, caspase-8 will lead to the proteolytic activation of caspases-3 and 7, leading to apoptosis [24].

In the intrinsic or mitochondrial pathway, the mitochondria releases to the cytosol several apoptotic proteins such as cytochrome C, apoptosis-inducing factor, and endonuclease G. The latter two proteins move to the nucleus mediating chromatin condensation and DNA fragmentation, independently of caspase signaling. Cytochrome C, on the other hand, will originate the formation of the apoptosome which, in turn, activates the initiator caspase 9. This initiator, like caspase-8, activates caspases-3 and 7, which trigger apoptosis. Another mechanism is the destruction of the anti-apoptotic protein Bcl-2 present in the endoplasmic reticulum and mitochondria [24].

Apoptotic cells also release signaling molecules into the extracellular environment that attract phagocytic cells, which are in charge of removing the resultant apoptotic bodies, preventing inflammation and the subsequent activation of the immune system. The requirement that the necessary complicated cellular machinery remains functional, which may not be the case after more aggressive PDT treatments, explains why less intense PDT protocols favor cell death by apoptosis [25].

1.2.3.2 Necrosis

Necrosis is a type of fast degeneration of relatively large cell populations that is characterized by cytoplasmic expansion, organelle destruction, and cell membrane disintegration. This extracellular release of cytoplasmic contents and pro-inflammatory mediators results in the emergence of a local inflammatory response [26].

More aggressive PDT methods with high PS and/or light dosages, as well as PS that tend to concentrate in cell membranes, likely to favor this pathway. Necrosis has been referred to as an uncontrollable and passive method of cell death. There is evidence, though, that signal transduction pathways associated with the mitochondria, that can be related to apoptotic pathways and have definite molecular effectors, can also initiate necrosis. The extent of mitochondrial damage appears to dictate the mode of cell death, with damaged mitochondria that are unable to produce ATP favoring necrosis [23]. As a result, controlled necrosis, a novel theory of cell death, was developed [27].

The processes of cell death induced by PDT primarily depend on the cellular structures that are directly impacted by oxidative stress. It appears that the autophagic pathway can be turned on as a defense mechanism by the cell to recycle the damaged proteins and structures in an effort to reduce oxidative damage. When cellular repair becomes impossible at a certain level of damage, the apoptotic pathway is activated. Necrosis becomes the only method for cell death when the PDT regimen is particularly aggressive, resulting in the destruction of the cellular machinery required for autophagy and apoptosis and the loss of cell integrity [23].

1.2.3.3 Autophagy

Autophagy is a catabolic mechanism initiated in eukaryotic cells that allows cell survival by removing toxic metabolites, pathogens, or damaged organelles. However, it can also promote cell death by degradation of cellular constituents and by autodigestion [23]. This mechanism starts with the formation of a double membrane that sequesters cytoplasmic components and organelles, subsequently forming autophagosomes. The outer membrane of the autophagosome fuses with a lysosome, originating an autolysosome that contains hydrolysomes that degrade its contents [23, 28]. The contribution to cell death is still uncertain, since under certain conditions, autophagy functions as a repairer of damaged cells, when apoptosis is the most present mechanism, allowing a reduction in the effectiveness of therapy. On the other hand, when apoptotic cells are destroyed by PDT, there is an increase in autophagic activity leading to tumor destruction. However, the mechanism responsible for the protective and the destructive activity is still unknown [28].

1.2.4 Photodynamic therapy-induced destruction of Tumor Vasculature

The enhanced vascularization that takes place in tumor tissues is one of the characteristics of a tumor that allows it to survive, grow and disseminate through the organism. This occurs as a result of tumor cells secreting more Vascular endothelial growth factor (VEGF), which causes the tissue to neovascularize. This is a crucial process used by tumors to enhance blood flow into the growing tissue. Without this phenomenon, the tumor would not obtain enough oxygen, nutrients, and space to expel metabolic waste products. PDT makes use of this circumstance. Some PS may accommodate in the walls of the tumor vasculature after PS injection. The PS absorbed by the tumor vasculature's endothelial cells will go through a similar activation mechanism when exposed to radiation. As a result, the blood flow to the tumor tissue will be disrupted and the blood vessel walls will be destroyed. The dense tumor tissue will then have limited nutrition and oxygen and will accumulate metabolic waste products from the cell metabolism [29, 30].

Contrary to standard cancer treatments, tumor cells have been shown to alter their metabolism in order to survive and proliferate in a hypoxic environment. The chemokines, cytokines, and juxtracrine cell contacts in the tumor microenvironment will change, stimulating the nearby normal cells, like fibroblast and endothelial cells, for survival sustenance. This causes fibroblasts to differentiate into cancer-associated fibroblasts, creating ECM for the tumor cells. This results in tumor recurrence and therapy resistance [31, 32].

1.2.5 Immune System Activation Following Photodynamic Therapy

The ability of tumors to avoid immunological detection by immune system cells is another significant characteristic that helps them survive inside the body. Pathological antigens that the immune system must be able to recognize are hidden from immune response when cancer develops. This happens through a variety of processes, including the production of molecules that inhibit immune cells from initiating an immunological response and the presentation of surface molecules that have similar effects [33]. The actions of PDT directly activate the immune system [34].

Tumor necrosis factors (TNFs) and cytokines are released as a result of cancer cell death and release of cellular debris, which exacerbates inflammation and starts a chain reaction of other immune response mechanisms [35]. Leukotrienes, acute phase proteins, complement system components, histamine, granulocyte colony-stimulating factors, prostaglandins, and numerous other chemical mediators of inflammation and immunological reactivity are also released post-PDT cytotoxicity [36]. Additionally, after treatment, dying tumor cells release molecules into the vascular system, such as alarming and damage-associated molecular patterns (DAMPs) that activate the innate immune system [27, 37]. Innate immune system cells, including macrophages, dendritic cells (DCs), natural killer (NK) cells, lymphocytes, and particularly neutrophils, are then activated as the cancer cells' mechanism of escaping detection has been compromised.

Therefore, PDT causes not only inflammation but also immunogenic cell death. After innate immune responses activation, there is also stimulation of the adaptive immune response. Helper T cells, cytotoxic T cells, and regulatory T lymphocytes are some of the cells of the adaptive immune system that are produced by antigen-presenting cells (APCs). This occurs as a result of a process that activates the adaptive immune system to support the innate immune system's function. Interestingly, the stimulation of the adaptive immune system causes the creation of a long-lasting antitumor immunity that inhibits tumor spread and prevents cancer from returning after PDT [38].

1.2.6 Photodynamic therapy as a clinical modality for cancer therapy

PDT has a number of benefits over traditional cancer therapy methods. Skin photosensitivity is increased by first-generation PS. However, when used properly, PDT has very few long-term negative effects. It can be done without anesthesia and is less intrusive than surgical techniques. PDT can significantly induce tumor death by destroying the surrounding vasculature in addition to the tumor itself [54]. The innate ability of some PS to preferentially concentrate in tumor tissue and light irradiation only in the target tissue are the two key elements that affect PDT's selectivity [39, 40]. Moreover, by using approaches to improve PDT selectivity, such as nanotechnology, it is possible to use it precisely and directly to the target tissue with minimum systemic side-effects [39].

In contrast to radiation, PDT can be performed repeatedly in the same area. After recovery, there is little to no scarring. Additionally, it is typically less expensive than other therapeutic methods for the treatment of cancer [54,55]. Similar to all therapeutic techniques,

PDT has potential drawbacks. With the current state of technology, the photodynamic action only manifests itself selectively in the irradiated site, making its application to widespread metastases highly challenging [39].

Ineffective PDT can result from tumors surrounded by necrotic tissue or dense tumor masses since the photodynamic impact depends on tissue oxygenation. The most crucial factor when considering PDT as a therapeutic option is the precision of target tissue irradiation. Due to the poor penetration of visible light into the tissue, deep tumors (which are difficult to approach without surgical intervention) are difficult to treat [39, 41]. The advantages and disadvantages of PDT are summarized in Table 1.

1.3 Photosensitizers

PS are compounds that may absorb light of a certain wavelength and cause photochemical or photophysical processes. In addition to light and oxygen, PS are one of the three essential components of PDT. PS can be either natural or manufactured. The capacity of PS to absorb light at a specific wavelength and produce ROS enables PDT to cause chemical or physical damage in the target cancer tissues [42].

Table 1 - Advantages and disadvantages of PDT in cancer

	Advantages	Disadvantages
	✓ Less adverse side effects	Photosensitivity following
	✓ Minimal intrusion.	therapy.
	✓ Short healing time.	✗ The precise delivery of light to
	✓ Available for use in	the tumor is essential for
	outpatient settings.	successful treatment.
PDT for cancer	✓ Can be used repeatedly in	✗ For the photodynamic impact to
· ·	the same area.	occur, tissue oxygenation is
	✓ A little scar, if any, following	essential.
	healing.	 Metastatic malignancies cannot
	✓ Less expensive than	be treated with present
	alternative therapies.	technologies.

As with any class of medication, there are a number of qualities and circumstances that define the optimum PS [43-45].:

- Very high chemical purity.
- Minimal cytotoxicity in the dark;
- Photosensitivity in the presence of a specific wavelength.
- High photochemical reactivity;

- Minimum absorption in the 400–600 nm range, limiting sunlight photosensitivity
- Stability at ambient temperature.
- The absorption bands should not overlap the absorption band of other chemicals in the body (such as melatonin, hemoglobin, or oxyhemoglobin).
- Simple solubility in body tissues.
- High selectivity for tumor tissues: The PS should be gradually withdrawn from the treated areas, remaining there for at least a few hours, but be promptly eliminated from healthy tissues, phototoxic systemic effects.
- Low cost, straightforward synthesis, and accessibility.

1.3.1 Light

For PDT to be effective, the use of a suitable light source is necessary. The effectiveness of the therapy will depend on whether the emission spectrum of the light source matches the absorption spectrum of the PS [46]. Furthermore, the greater or lesser tissue penetration of a given light source is also very important, with light with a wavelength corresponding to the red or infrared zone being more penetrating. For wavelength values between 600nm and 1200nm lies the so-called optical window of the tissue [47]. However, not all wavelengths within this optical window are able to trigger a photodynamic effect, as energy transfer is required for oxygen to switch from the normal to the singlet state, which is only possible with the use of light sources with a wavelength up to 850nm. Taking these factors into account, it is also necessary to determine the PS action spectrum, which describes the relative efficacy for different wavelength values [46].

Currently, light sources used in PDT belong to three major groups: broad spectrum lamps, diodes and lasers [19], and one should always take into account the total fluence of light to be applied, which consists of the energy rate applied to the biological tissue, the fluence rate, the exposure time as well as the mode of delivery of the light source [47]. Broad spectrum lamps in the early application of PDT were widely used due to their low cost and easy handling, but on the other hand, their coupling to optical fibres to deliver light to internal organs without decreasing efficacy is difficult [18].

Lasers and led have made a significant contribution to improve the conditions for PDT [18]. Although LASERs are expensive, they do offer some benefits, such as monochromaticity and high efficiency (>90%) of coupling into single optical fibers in endoscopic, high potency, and interstitial light delivery systems. One of the most affordable LASER systems is diode laser. It is extremely practical and efficient, but because each photosensitizer absorbs light at a different wavelength, a separate unit is needed for each one. In the past several years, LED has emerged as a practical PDT technique, particularly for irradiating tissue areas that are easily accessible. Due to their low cost and simplicity of construction into various irradiation configurations, LED sources may be beneficial over LASER or diode LASER sources. Although

LEDs have a fixed output wavelength like LASER diodes do, having separate sources for each photosensitizer is less of a disadvantage because of the lower cost per watt [48].

1.3.2 Generations of Photosensitizers

Currently, PS employed in PDT are categorized based on the conceptual frameworks and historical developments of first, second, and third generation PS.

1.3.2.1 First generation

Despite having a wide range of uses, first generation PS (the main example being HPD) have some clinical application restrictions due to poor tissue penetration caused by maximum absorption at a relatively short wavelength (630 nm) and low chemical purity. In addition, since PS have a long half-life and accumulate highly in the skin, skin hypersensitivity reactions to light may occur for several weeks following PDT. Due to the drawbacks of the first generation of PS, research on other compounds has been carried out, which led to the creation of the second generation of PS [49, 50].

1.3.2.2 Second generation

Studies on the upcoming class of PS started in the 1980s. Only a few of the several hundred compounds with prospective photosensitizing characteristics had been employed in clinical trials. Even fewer chemicals have been formally licensed for use in clinical anti-cancer PDT. Hematoporphyrin derivatives and synthetic PS like 5-aminolevulinic acid, benzoporphyrin derivatives, texaphyrins, thiopurine derivatives, chlorin, as well as bacteriochlorin analogues and phthalocyanines are currently included in the group of the second-generation PS [16, 51].

Due to their maximal absorption in the wavelength range of 650–800 nm, higher chemical purity, a higher yield of singlet oxygen production and improved penetration to deeply positioned tissues, second-generation PS have a higher potential for PDT applications. They also exhibit less side-effects due to a stronger selectivity for malignant tissues and a quicker removal of the PS from the body. The fundamental drawback of the second-generation PS is that they are poorly soluble in water, which severely restricts their intravenous administration and highlights the need for the development of novel drug delivery strategies [43].

1.3.2.3 Third generation

The production of molecules with a higher affinity towards tumor tissues, which lessens harm to nearby healthy tissues, forms the basis for the third generation of PS. The challenge of developing a pharmacological process that would allow the parenteral injection

of PS is another obstacle to the widespread clinical application of PDT in oncology. The bioavailability of several PS is being effectively increased by new drug delivery [52]. The following photodynamic treatment adjustments are utilized to improve the PS selectivity [52, 53]:

- Combining receptor-targeted compounds with second-generation PS;
- Combining PS with low-density lipoproteins since multiplying tumor cells require more cholesterol for the formation of cell walls;
- Combining PS with antigen-specific monoclonal antibodies that target cancer cells;
- The utilization of hormones, transferrin receptors, or growth factor receptors as tumor surface indicators.

The improvement of the selectivity and PS accumulation in the affected areas, given by these approaches provides the potential of lowering drug dosages while maintaining the efficacy of the treatment [52, 53].

In addition, ongoing studies focus on the development of fourth generation PS, for this a third generation PS is used and added with an encapsulated small molecule inhibitor capable of blocking tumor survival pathways after PDT treatment to increase its general efficacy in clinical settings and thereby prevent potential tumor recurrence. Currently, the use of PDT and inhibitor combinations in clinical settings is restricted to the treatment of macular degeneration, in which VEGFs inhibitors are used to prevent tumor neovascularization [52].

1.3.3 Verteporfin as a photosensitizer

Verteporfin (VP) $(C_{41}H_{42}N_4O_8)$ is a derivative of a protoporphyrin, containing a benzoporphyrin monoacid ring A, with a strong absorption peak at 690 nm (Figure 3) [54].

As a result of its poor cancer cell selectivity, this drug was quickly repositioned in the ophthalmology sector for AMD therapy after local administration. It was originally developed as an efficient PS for the control of cancer by PDT. FDA certification of Visudyne® for the latter therapeutic purpose came in 2000. VP limitations include poor water solubility and limited biopharmaceutical performance, along with limited tumor selectivity. In this context, nanotechnologies may broaden its pharmaceutical and medical performances, ranging from improved the drug pharmacokinetics to ameliorated selectivity and ability to mitigate tumor resistance [54].

1.3.3.1 Verteporfin discovery and development

The discovery of VP is linked to the need to employ new PS to sharpen and improve tumor treatment through PDT. It is a chlorin-type molecule with high chemical stability which

can produce singlet oxygen with high efficiency [66]. It possesses every theoretical attribute required for an efficient PDT. As a result, low power light non-thermal laser at wavelengths that can pierce through fibrotic tissue, blood, and melanin can be used for its activation, [55].

Some studies have shown that compared to less recent PS, such as hematoporphyrin, VP have a 4 times more effective light absorbing at 700 nm, a suitable wavelength for tissue penetration. Therefore, VP can induce a much higher cytotoxicity than hematoporphyrin (10 times more phototoxic in human adherent cell lines) [55].

Due to these characteristics, VP has emerged as a viable and secure PDT candidate for the treatment of cancer. Today, when paired with molecular vehicles or loaded into nanocarriers, VP can be categorized into the third generation PS [56, 57]. Since VP is a

Figure 3 - Chemical structure of Verteporfin

hydrophobic molecule, it was first loaded into liposomes. Clinical studies on the VP liposomal formulation have identified novel therapeutic alternative applications [57, 58]. In fact, research in 1993 showed that the newly developed lipid-based VP formulation was the ideal choice for PDT to treat the newly developed choroidal neovascularization within the retina brought on by AMD [59, 60]. The retina is severely damaged by AMD, a common illness that results in visual loss as a result of genetic and environmental causes [61]. PDT for AMD includes injecting VP, which builds up in the aberrant capillaries of the eye and is locally activated by nonthermal light (693 nm), intravenously. In an interaction with oxygen, the activated VP produces cytotoxic singlet oxygen and free radicals that damage vascular endothelial cells and cause platelet aggregation, activation of the clotting cascade, and microvascular occlusion [62].

Twenty eight clinical facilities in Australia, North America, and Europe participated in VP clinical trials. The purpose of the Phase I/II study was to assess the therapeutic efficacy of VP as well as the potential for systemic or localized adverse effects and safety concerns. The successful completion of Phase III studies in accordance with the Treatment of AMD with PDT protocol, developed through negotiations with the FDA and European regulatory authorities, was made possible by the positive outcomes. VP was approved under the name Visudyne® in Switzerland at the end of 1999, and in the European Union and the United States in 2000, as a result of the excellent results attained. VP is currently the gold standard treatment for AMD [60].

1.3.4 Cancer treatment using verteporfin

PDT is mostly employed clinically to treat AMD [14]. After systemic delivery of a non-toxic PS agent, PDT causes the localized death of tumoral or dysfunctional tissues and vasculature through photochemical and photophysical reactions that culminate in the production of ROS. In cases where a portion of the tumor was only partially removed, PDT can be employed. Consequently, VP has been carefully examined for its extraordinary qualities as second-generation synthetic PS for PDT in solid tumors in addition to the excellent results of the AMD treatment [63].

VP has several beneficial characteristics for the treatment of solid tumors. After systemic administration, VP reaches the peak of tumor tissue concentration in 1-2 h, reducing the risk of skin photosensitivity (by 24 h), as it is quickly excreted into bile. In addition, it is triggered by exposure to light with a wavelength of around 690 nm, which profoundly penetrates tissues. Additionally, VP interacts with plasma lipoproteins such low density lipoproteins because of its hydrophobic nature. Because some proteins mediate VP transport, this circumstance may be beneficial for tumoral PDT applications. More specifically, these low density protein receptors are overexpressed in tumor cells and vascular endothelial cells that are associated with tumors [64].

Presently, VP-mediated PDT is being assessed in a number of oncologic clinical investigations. PDT with VP is safe and effective, according to the findings of Phase I/II clinical trials for the treatment of locally advanced pancreatic tumors [65]. Phase I/II of the PDT with VP clinical investigations for the treatment of primary breast cancer revealed additional favorable results. PDT with VP demonstrated to be a promising, secure, and minimally invasive treatment with few side events when compared to traditional therapies even when used under imaging guidance [63]. Despite preferentially accumulating in tumor tissue, lipophilic PS are not truly tumor-selective substances. One popular strategy to get around this problem is to select molecules that are overexpressed in tumors and use them as PS targets. A recent study used the high expression of the Heat shock protein 90 on the surface of breast

cancer cells as an exploitable target, leading to the development of a promising selective agent for cancer PDT through the conjugation of VP and the protein small molecule inhibitor.

In this respect, the use of nanotechnological approaches is increasing the selectivity, stability, and biopharmaceutical performances of VP PS-based drugs [64].

1.3.5 Challenges of photodynamic therapy

Although PDT cancer therapy has several advantages, it is currently not usually properly adapted in clinical situations [42]. The majority of PDT clinical setting limitations are related to several of the first and second generation PS drugs inherent properties including their solubility, method of delivery, and targeted tumor tissue selectivity [39, 66]. Maximum levels of ROS formation are necessary to ensure the overall efficacy of PDT in terms of triggering total cell death and complete tumor destruction, and this is strongly dependent on the concentration level and uptake of a PS in cancer cells [67].

Since only small amounts of PS drugs are able to passively accumulate in tumor locations (due to the enhanced permeability and retention effect), non-targeted traditional PS drug delivery systems typically have a poor PDT clinical outcome. The remaining photosynthetic medication is either metabolized by the immune system or distributes into healthy tissues, where it might have undesirable side-effects such patient photosensitivity or localized healthy tissue damage [68, 69].

Additionally, the majority of second and third generation PS are hydrophobic and have a restricted water solubility, which causes them to agglomerate after administration and reduces ROS generation. This is a problem that frequently arises in clinical settings. Additionally, only cells that are adjacent to the proximal location of ROS formation, or PS localization, are directly impacted by PDT since ROS have a limited half-life. Additionally, singlet oxygen has a very narrow radius of effect. Because of this, the bioavailability of a PS and its extracellular and intracellular localization, as well as the overall extent of PDT-induced cytotoxicity and photodamage, are also crucial. Additionally, the majority of PS suffer from issues such as bioavailability, biodistribution, target specificity and poor water solubility. To assure PS aqueous solubility, with higher tumor selectivity PS drug nanocarriers are now being studied [68, 69].

In order to increase the effectiveness of PDT cancer treatment, PS selective delivery in tumor cells is a key aspect in studies on drug absorption. Therefore, current research work is focused on creating efficient PS-based third generation drug delivery systems. These targeted drug delivery strategies should more efficiently solubilize and transport the PS within the human body to actively target and accumulate in tumor cells and tissues with the least amount of harm and toxicity to normal tissues. They should also promote maximum ROS generation within tumor cells for a successful PDT [68, 70].

VP in particular has also several limitations that limit its widespread clinical use. It is a highly hydrophobic small molecule, meaning that it has limited solubility in aqueous solutions, making it challenging to be administered without excipients that could have negative side-effects. Therefore, the problem of solubility has to be further addressed in order to employ VP as a viable treatment [71]. This poor solubility and is high tendency to aggregate in aqueous media lead to another limitation, since only monomeric species are highly active. Therefore, this aggregation significantly lowers its therapeutic effectiveness. Despite the fact that this PS accumulates in cancer cells at higher amount due to the EPR effect, it also tends to be taken up by healthy cells in significant quantities, which may lead to issues of toxicity in healthy tissues. Thus, it is also important to evaluate porphyrins' cytotoxicity against healthy cells and develop strategies to improve tumor selectivity and minimize healthy tissue accumulation [72]. In this context, the development of VP-loaded nanoparticles may provide an innovative strategy for intravenous delivery of VP that can prolong its circulation time and enhance VP cancer cell selectivity [73].

1.4 Nanotechnology role in Photodynamic therapy

Nanotechnology, which is now applied in many fields of research, including medicine, appears to be a promising and rapidly evolving discovery of the twenty-first century. The National Nanotechnology Initiative defines it as using structures with a minimum size of 1–100 nm in at least one dimension [74].

In medicine, NPs are being used as delivery systems for targeting of specific cells or as agents in medical imaging. The primary characteristic that distinguishes NPs from bulk materials is their size, which has an impact on their biological mobility, energy absorptions, and chemical reaction. Additionally, NPs offer a number of benefits, including [74]:

- Enhanced drug delivery to tumor cells, which increases their anti-tumoral
 effectiveness, while limiting the accumulation and subsequent toxic effects on healthy
 cells.
- Enhanced drug half-live.
- Improved water solubility of hydrophobic drugs
- Increased drug permeation across biological barriers
- Improvement of the drug bioavailability.

Treatment of diseases, such as neoplasms, can be done more quickly and effectively due to the use of NPs in biology and medicine. As a result, the area of oncology has been and still is being impacted by the development of nanotechnology, raising the possibility of adopting new, creative medicines. The synthesis of NPs opens up the possibility of delivering active medication molecules to cells more precisely and accurately in order to achieve desired effects while minimizing negative effects. The majority of obstacles to medicine delivery were removed as a result of these operations. The ability of NPs to act as a form of medicine has also

been demonstrated. Numerous research teams have been studying the use of NPs in PDT for many years as they create new treatments [39, 75].

1.4.1 Enhancing Photosensitizers Delivery using Passive or Active Targeting Strategies

Due to their ability to counteract some of the drawbacks that traditional PS encounter in clinical settings, nanotechnology has been employed in combination with PDT [76]. NPs can considerably boost the PS passive cellular uptake via the EPR effect [70]. This effect allows the NP drug carriers to cross the larger pore sizes that are present in the vasculature of tumor cells. Additionally, a limited lymphatic filtration increases the accumulation of the PS in the tumor region [70].

Actively functionalized PS drug delivery systems, however, are the current hot area of research because the ultimate goal of PDT is to selectively eliminate cancer cells with little collateral harm to surrounding normal healthy tissues. Thus, research studies have been conducted to further functionalize PS drug delivery systems by attaching particular active targeting moieties (biomolecules or ligands) such as antibodies, peptides, or aptamers to their surface in order to improve tumor PS uptake selectively and sub-cellular localization [76, 77]. These moieties have a particular affinity for particular receptors that, contrary to normal cells, are only overexpressed in the tumor cells. This is known as direct active targeting, while the targeting of the tumor vasculature is denominated indirect active targeting. This surface functionalization of PS drug delivery systems makes it easier for PS to accumulate and become subcellular in tumor tissues or cells in a more effective, specific, and active manner, which increases PDT's overall effectiveness with less harm to healthy, normal tissues [49, 76, 77].

Many different organic and inorganic nano-platforms have been investigated up to this point for effective and focused PS medication delivery. Since NPs can overcome some of the difficulties that conventional PS drug delivery have in terms of stability, solubility and tumor selectivity, they also increase the effectiveness of PDT [9, 77].

Inorganic NPs include ceramics, that have good biocompatibility and allow surface functionalization. magnetic and metallic NPs, which may have superparamagnetic properties and can be used in theranostics, quantum dots, which can also be used as PS, having broad excitation and limited photobleaching, among others [66].

Solid organic materials such as lipids, proteins, polysaccharides, or polymers can be used for the production of organic NPs [78]. Liposomes, polymeric NPs (such as albumin, hyaluronic acid, chitosan, hydrogels, polymeric micelles, dendrimers, biodegradable polymers, and hyperbranched polymers), as well as protein-based NPs (such as albumin, amino acids, gelatin, collagen, silk, and peptides) are examples of organic NP platforms already studied for PDT applications [79, 80]. For the purpose of ensuring controlled and safe

delivery, different PS have been strategically loaded into these types of NP with very encouraging results [78, 79].

To improve biocompatibility, stabilize, and allow the PS-loaded NPs to circulate for longer periods of time inside the organism, NPs may be covered with a polyethylene glycol (PEG) shielding outer layer. To functionalize the surface of nanoplatforms, tumor targeting ligand agents can be used, including monoclonal antibodies, aptamers, nucleic acids or small molecules like peptides or their fragments. These homing ligands are linked to the surface of NPs, allowing for active targeting of specific receptors overexpressed in cancer cells, including, epidermal growth factor receptors (EGFR), folate receptors (FR), transferrin-receptors (TfR), CD44, and many others, which improves PS cellular uptake [81]. One interesting example if the targeting of the FR overexpressed in tumor cells. Folic acid (FA) is a water soluble vitamin B molecule used for DNA synthesis and repair. Given its low cost, simple nanoparticle conjugation, little immune system activation, and minimal impact on the pharmacokinetics of the nanocarrier, FA surface functionalization is an appealing method for cancer active targeting [82].

Overall, the use of NPs provides a flexible platform for PS delivery by passively or actively targeting tumor cells. Most of these NPs benefit from minimal toxicity and could increase the solubility of the PS as well as their accumulation within the target tumor site. Moreover, they could provide additional benefits in the context of PDT, such as improved light penetration and up-conversion of low-energy radiation into high-energy emission, which speeds up the PDT destruction process in deep-seated tumors [9, 78, 79].

1.4.2 Lipid nanoparticles

Lipid nanoparticles are colloidal carriers with a lipid matrix that are solid at both room and body temperature. They were developed in the 1990s as an alternative to polymeric NPs, liposomes, and emulsions [83]. Lipid nanoparticles are composed of lipids, most of them classified as generally recognized as safe (GRAS). Those include fatty acids, fatty esters, fatty alcohols, triglycerides or partial glycerides, and waxes. These lipids are stabilized in aqueous solution by surfactants, such as polysorbate 80, which reduce the surface tension between water and lipids [84, 85].

For pharmaceutics and cosmetics applications, the use of lipid solid matrix as drug carriers has a high potential since it allows for a controlled release and site-specific targeting of active ingredients. Additionally, they exhibit good stability *in vivo*, offer improved drug solubility, and effectively incorporate and distribute drugs that are both hydrophilic and lipophilic via parenteral and non-parenteral modes of administration [84, 86].

In addition to having good tolerability due to the biocompatible and biodegradable nature of the ingredients utilized, lipid nanoparticles composition is based on commercially available lipids and surfactants that have received FDA approval. Additionally, their manufacturing procedure is inexpensive and simple, which facilitates their production in large-scale [85, 86]. In addition, some of the production methods do not require the use of organic solvents [85, 86].

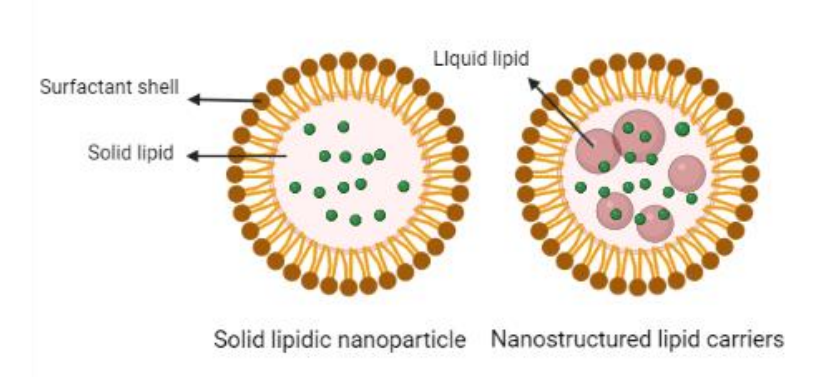


Figure 4 - Schematic represent of lipid nanoparticles, including SLN and NLC

1.4.3 Solid lipid nanoparticles and nanostructured lipid carriers

Solid lipid nanoparticles (SLN) are the first generation of lipid-based nanocarriers. These NPs are created by dispersing 0.1 to 30% (w/w) of solid lipids in an aqueous media and, if necessary, stabilizing them using a surfactant [87]. As a result, a well-structured matrix with just a few cavities for drug encapsulation is assembled.

SLN can be divided into three drug inclusion models based on where the drug is located inside the structure. In the solid solution model, the drug is dispersed in the lipid matrix and has strong interactions within the lipid core. The second model, known as the drug-enriched shell model, describes how drug molecules concentrate on an outer shell that is produced when a drug-free lipid core is present at the surface of SLN and when the drug concentration is near to its saturation solubility in lipid, which will result in its precipitation in the core and the creation of a lipid covering [88].

Solid lipids such as mono-, di-, or triglycerides, fatty acids, and complex glyceride mixes are employed as the main component and mixture of polymers or surfactants stabilizes this lipid matrix. Site-specific targeting, physical stability over an extended period, the potential for regulated release of both hydrophilic and lipophilic pharmaceuticals, protection of labile chemicals, low cost, simplicity in manufacturing, and nontoxicity are just a few of the many benefits of SLN. In contrast, SLN have some drawbacks, including a limited capacity for drug loading and drug expulsion as a result of crystallization under storage conditions [89].

Nanostructured lipid carriers (NLC) are the second generation of lipid nanoparticles, developed to overcome some of the limitations of the SLN In fact, the core of NLC differs from

SLN due to the presence of both solid and liquid lipids, which improves the drug entrapment and limits drug leaking during storage, by creating a more disordered lipid matrix with cavities where the drug can more easily accommodate [90].

1.4.4 Production methods

Numerous different methods for the production of lipid nanoparticles have been reported in the literature. The choice of the appropriate method is done according to the composition and the desired characteristics of the lipid nanoparticle, as well as the properties of the drug [91]. Some the most common synthesis methods for lipid NPs are described below.

1.4.4.1 High pressure homogenization

High-pressure homogenization (HPH) technique represents one of the most common methods established for the production of lipid NPs. This procedure involves applying high pressure to a liquid containing the drug's active ingredient and a lipid via a micron-sized gap, either at high temperature (hot homogenization) or below room temperature (cold homogenization), to produce submicron-sized particles. The drug is first dissolved or dispersed in the lipid, which has already been melted at a temperature 5-10° over its melting point, in both situations [92].

In the hot homogenization the lipid-drug melt is dispersed in a hot surfactant solution and then passed through an HPH to form the emulsion that will recrystallize forming the NPs, after cooling down. In contrast, the cold homogenization is carried out following the solidification and breakdown of the drug-containing melted lipid into microparticles, which are then suspended in a cold surfactant and then subjected to the HPH at room temperature. This process results in the formation of solid lipid nanoparticles. The use of temperature-sensitive drugs, unintended drug distribution into the aqueous phase during homogenization, and the complexity of the nanoemulsion crystallization step, which can result in significant modifications, are just a few of the limitations associated with the process at high temperatures that the cold HPH solves [93].

The cold HPH overcomes some limitations regarding the process at high temperatures such as the use of temperature-sensitive drugs, the unintentional drug dispersion into the aqueous phase during homogenization and the difficulty of the nanoemulsion crystallization stage, which might significantly alter the final product [92].

1.4.4.2 Microemulsion technique

The microemulsion technique allows the production of SLN dispersions by precipitation from a heated microemulsion, a thermodynamically stable system comprising water and a lipophilic phase, stabilized by surfactants and optionally co-surfactants [91].

Melted lipids are combined with water and surfactant that have been heated to the same temperature before being gently mixed. The lipid droplets harden as the generated microemulsion is then disseminated in a cold aqueous media while being gently mechanically mixed.

1.4.4.3 High shear homogenization and ultrasonication technique

Ultrasonication and high shear homogenization are dispersion methods. The melted lipid is dispersed by high shear homogenization followed by ultrasonication in the warm aqueous phase that contains surfactants to produce the lipid NP dispersions. The emulsion's droplet size is reduced by sonication, and a lipid NP dispersion is produced by gradually cooling the heated emulsion [92].

1.5 Aims and objectives

The objective of this research is to create an innovative two-stage treatment that combines light energy with the PS VP encapsulated into SLN, designed to destroy cancer cells after light activation (PDT). The encapsulation of VP was performed with the main goals of improving its pharmacokinetics by enhancing its water solubility and improve its tumor targeting ability, aiming to lower the drug's non-specific accumulation, and systemic adverse side effects.

To do so, VP-loaded SLN were produced and functionalized with FA to target the FR, which is a recognized biomarker for tumor cells due to its overexpression on a large number of tumors [94]. A detailed physicochemical characterization and stability study of the NPs was then carried out. Additionally, the hemolytic activity of the nanosystem was evaluated, aiming to verify the suitability of the nanoformulation for intravenous administration. Moreover, the cytocompatibility of the nanosystem in dark conditions was evaluated in the reference cell line L929. The PDT efficacy of the nanosystem was then assessed in the human breast cancer cell line MCF-7 (used as a proof of concept), combining the PS with a LED light source at 690 nm. Following an optimization of the different parameters of the light irradiation experiment, the different nanoformulations and free VP in both dark and light conditions were evaluated in their capacity to elicit cancer cell death. Additionally, the NP targeting ability, the production of ROS and induction of cancer cell apoptosis with and without light irradiation were also investigated.

2 Chapter Materials and Methods

2.1 Materials

Cetyl Palmitate was kindly provided by Gatefossé (Gatefossé, France). Verteporfin, Tween® 80, Triton™ X-100, Trypan Blue powder, Folic Acid, Triethylamine, dicyclohexylcarbodiimide, N-hydroxysuccinimide, Sodium chloride, 2′,7′-Dichlorofluorescin diacetate, Dimethyl sulfoxide (DMSO), Resazurin sodium salt, Dulbecco's Phosphate Buffered Saline 10X (PBS), Formalin solution neutral buffered 10%, and 2′,7′-Dichlorofluorescein diacetate (DCFDA) were obtained from Sigma-Aldrich® (St Louis, MO, USA). Chloroform, Dulbecco's Modified Eagle's Medium (DMEM), 0.25% Trypsin-EDTA (1X), Penicillin-Streptomycin (Pen Strep), and Heat Inactivated Fetal Bovine Serum (FBS) were purchased from Gibco® by Life Technologies™ (UK). Hoechst 33342® Trihydrochloride Trihydrate were obtained from (Invitrogen, Thermo Fisher Scientific, MA, USA). FITC Annexin V Apoptosis Detection Kit with 7-AAD was purchased from Biolegend® (California, USA). MCF-7 (passages 77-90) was purchased from ATCC (Middlesex, UK). L929 cells (passages 18-24) were obtained from Cell Lines Service (CLS, Eppelheim, Germany). LS-LED LED Light Source with a 690 nm LED slide was purchased from Sarspec (Porto, Portugal)

All the weighting measurements were performed using a Kern ABT 120-5DM digital analytical balance (Kern & Sohn; Balingen, Germany). pH measurements were obtained using a Crison pH meter GLP22 with a Crison 52-02 tip (Crison; Barcelona, Spain). Ultra-pure water was purified by an Ultra-pure water system (18.2 M Ω cm, Healforce, Shanghai, China) by a reverse osmosis process.

2.2 Production of Solid Lipid Nanoparticles

SLN were produced using the hot ultrasonication technique as previously described [95]. Using the dispersing process known as hot ultrasonication, melted lipid-surfactant solutions in warm aqueous phases can be ultrasonically agitated to produce lipid NP dispersions. Sonication reduces the droplet size and the cooling of the hot emulsion results in the formation of a lipid nanoemulsion [92].

The formulation composition used for the production of the SLN was adapted from previous studies and comprises the solid lipid Cetyl palmitate (210 mg) and surfactant Tween® 80 (70 mg) [95]. The condensation of palmitic acid with palmityl alcohol produces the palmitate ester known as cetyl palmitate, which is FDA-approved [96]. The FDA has authorized the selected emulsifier Tween® 80 (Polysorbate 80), also known as polyethylene glycol sorbitan monooleate, for the delivery of injectable, oral, and topical medications. It is a non-ionic detergent that is often used as an emulsifier [97].

In this procedure the lipid phase was melted above the melting point of the solid lipid using a water bath at 70 °C (Variomag Electronicrührer, Labortechnik, Munich, Germany). After that, the aqueous phase (4.4 mL of ultra-pure water) pre-heated at the same temperature was added to the lipid melt, and ultrasonically processed to make the pre-emulsion droplets smaller using a probe sonicator (VCX130, Sonics and Material Vibra-CellTM with a CV-18 probe; 115 Newtown CT, USA) at 70% for 5 min. In order to produce SLN, the hot colloidal emulsion was cooled to room temperature. For the production of VP-loaded SLN, 5 mg of VP were dissolved in the lipid phase and then ultrasonically processed to create VP-loaded SLN.

The nanoformulations were then protected from light with aluminum foil (since VP is a light-sensitive compound) and stored at 4 °C for later use.

2.3 Synthesis of Disteroylphosphatidylethanolamine-poly (ethylene glycol)2000-folic acid (DSPE-PEG2000-FA) Conjugate

The synthesis of Disteroylphosphatidylethanolamine-poly(ethylene glycol)2000 folic acid DSPE-PEG2000-FA has four main steps to compose this process: activation of Folic acid (FA), coupling to DSPE-PEG₂₀₀₀NH₂, purification and lyophilisation. First, 1 g of FA was dissolved into a mixture of 40 mL of anhydrous DMSO and 0.5 mL of triethylamine (TEA) and the mixture was stirred under anhydrous conditions in the dark overnight. The resulting solution was then mixed with 0.5 g of dicyclohexylcarbodiimide (DCC) and 0.52 g of Nhydroxysuccinimide (NHS) and stirred for 18h in the dark. To remove the precipitated side product dicylcohexylurea (DCU), the solution was filtered with a 0.45 µM filter. DMSO and TEA were evaporated under vacuum. After formation of NHS ester of folic acid (NHS-FA), the next step was coupling to DSPE-PEG₂₀₀₀-NH₂. This was done by addition of 2 mL of the solution containing activated FA to 50 mg of DSPE-PEG₂₀₀₀-NH₂dissolved in 1 mL of DMSO followed by overnight stirring in the dark under anhydrous conditions. After that, the mixture was evaporated under vacuum to remove DMSO and 6 mL of water were added. DSPE-PEG2000-FA conjugate was then dialyzed against 500 mL of ultra-pure water using a dialysis membrane (3.5 kD MWCO, SpectrumLabs, CA, USA) for 48h in order to remove unconjugated FA. Finally, the resulting solution was lyophilized using a freeze dryer (LyoQuest -85 plus v.407, Telstar). The obtained orange dry powder was stored at -25°C until further use [98, 99].

2.4 Production of Functionalized Solid Lipid Nanoparticles

Production of DSPE-PEG-FA functionalized SLN was performed by adding DSPE-PEG2000-FA to the lipid phase in a ratio of 1% w/w of the total lipid mass prior to the lipid melting.

2.5 Nanoparticle Characterization

2.5.1 Dynamic Light Scattering

A precise method for determining particle size and Polydispersity Index (PDI) is dynamic light scattering (DLS), also known as photon correlation spectroscopy. This method involves directing a laser beam through a suspension of particles, and then collecting the dispersed light in a detector. The time-dependent variations in the intensity of the scattered light are a result of the Brownian random motion of the particles in a liquid, and the diffusion coefficient of the particles can be found by analyzing these variations. The average hydrodynamic radius (dp), inversely proportional to the particles diffusion coefficients (D), is then estimated by the Stoke-Einstein relation, where k is the boltzmann constant (Equation 1) [100, 101]. The exact values of the liquid parameters temperature (T) and viscosity (η) must be known in order to determine the particle size accurately.

(Equation 1)

$$D = \frac{kT}{3\pi\eta dp}$$

A particle size analyzer (Brookhaven Instruments Corporation; Software: Particle Sizing v.5 Brookhaven Instruments; Holtsville, NY, USA) operating at a scattering angle of 90° and at room temperature, with dust cut-off set to 30 and refractive index of 1.33 was used to calculate the mean effective diameter size and PDI of the synthesized formulations. For each measurement, three runs of 2 min each were completed. Samples were diluted in ultra-pure water at a ratio of 1:400.

2.5.2 Zeta Potential

In a colloidal solution, particles frequently exhibit an electrical double layer made up of ions drawn to the particles by their surface charges. The produced bilayer is made up of an exterior region (diffuse layer) and an inner zone (stern layer), where the ions are less strongly connected to the particle surface as seen in Figure 5. The zeta potential is the potential that can be measured in a boundary when a particle acts as a single entity within the diffuse layer [102, 103]. Zeta potential is a measurement of surface charge and the electrokinetic potential of particles in colloidal systems. Along with cellular absorption and intracellular trafficking, it can affect particle stability[104].

Particles need to have strong enough repelling forces to avoid aggregation. It is well accepted that an electrostatically stable suspension requires a certain value of zeta potential (< -30 mV). If the zeta potential of the particles is lower, surfactants must be added to increase the electrostatic repulsions. Colloidal stability results from high positive or negative zeta potentials larger than 30 mV. Smaller than 5 mV levels, on the other hand, can cause agglomeration. Zeta potential is influenced by the nature of the solution, including pH and ionic strength, in addition to the characteristics of nanoparticles. Finally, the zeta potential may differ slightly from the surface potential of associated particles [104].

It is possible to measure the electrophoretic mobility of a suspension of particles using the analytical method known as electrophoretic light scattering (ELS), which uses the same fundamentals as DLS. The sample is exposed to laser light, and the dispersed light is collected

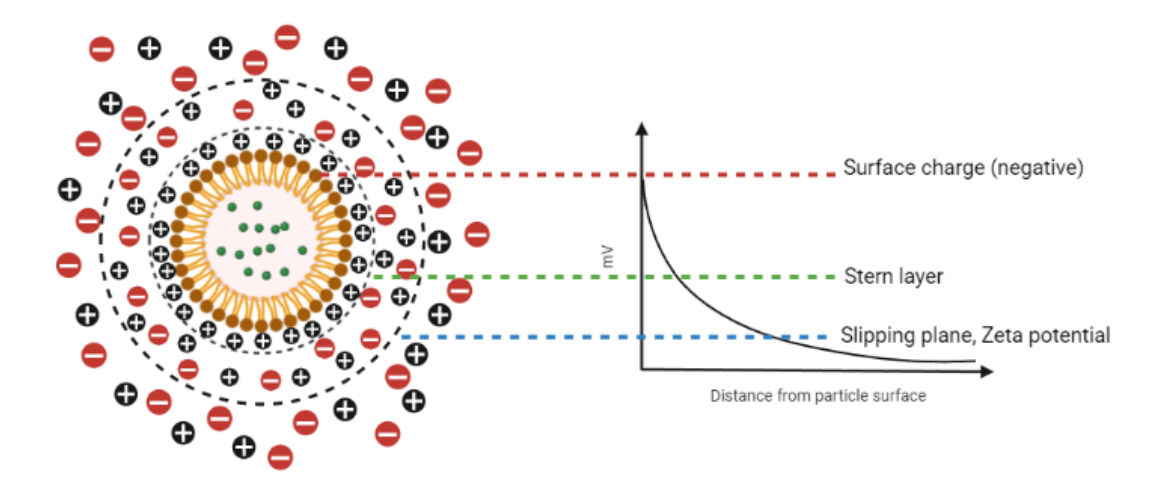


Figure 5 - Schematic representation of zeta potential (ζ)

using a photodetector. ELS, on the other hand, places two electrodes within the dispersion and generates a powerful enough electric field to ensure that electrokinetic activity prevails over random Brownian motion. Due to the particle charge-dependent migration that occurs with a particular velocity (mobility) towards the electrode that is oppositely charged, the frequency of the scattered light will change. Then, using the Henry equation , frequencies are converted into electrophoretic mobility, which is related to the particle zeta potential [102, 105]. The equation shown below represents Henry's equation for the electrophoretic mobility μ of a spherical colloidal particle of radius a with a zeta potential ζ , where ϵ_r relative permittivity of the medium, ϵ_0 permittivity of free space and $f(\kappa a)$ refers to Henry's function.

(Equation 2)

$$\mu = \frac{\epsilon_r \epsilon_o}{\eta} \zeta f(\kappa a)$$

An electrode and a Zeta Potential Analyzer (ZetaPALS, Brookhaven Instruments Corporation, Software: PALS Zeta Potential Analyser v.5, Brookhaven Instruments; Holtsville, NY, USA) operating at a scattering angle of 90° at room temperature were used to measure the zeta potential of each nanoformulation. At a ratio of 1:400, samples were diluted in ultrapure water. Six runs of ten cycles each were run for each measurement.

2.5.3 Encapsulation Efficiency

The determination of VP encapsulation efficiency (EE) was determined by UV-vis spectrophotometry, by determining the concentration of drug that was not loaded into the SLN.

In order to completely separate the SLN from the aqueous phase containing the free VP, formulations were centrifuged (Multifuge X1R, Thermo Fisher Scientific, USA) at 3900 rpm in centrifugal filter units (Amicon® Ultra Centrifugal Filters Ultracell-50 kDa, MERK Milipore, Ltd; Cork, Ireland) in the ratio of 1:65 using ultra-pure water for dilution (2mL).

Then the supernatant was removed and analyzed in UV-vis spectroscopy (Jasco V-660 Spectrophotometer, Software: Spectra Manager v.2, Jasco Corporation, USA) at 690 nm. This result was compared with the calibration curve of VP to calculate the EE of VP. This calibration curve of VP was prepared in ultra-pure water with 0.1% DMSO, using increasing known concentrations of VP.

The amount of VP present in the supernatant was subtracted from the original amount of VP added during the SLN production as shown by the equation below:

(Equation 3)

$$EE = \frac{Total\ amount\ of\ VP-Amount\ of\ VP\ in\ the\ supernatant}{Total\ amount\ of\ VP}$$

Loading capacity (LC%) can be calculated by the amount of total entrapped drug divided by the total nanoparticle weight. Yield in drug delivery measures the amount of drug delivered relative to the amount of drug encapsulated and is expressed as a percentage, as shown by the equation:

(Equation 4)

 $LC = \frac{\text{Total amount of VP} - \text{Amount of VP in the supernatant}}{\text{Total amount of lipid}}$

2.5.4 Stability study

To evaluate the stability of the formulations over time, periodic assessments of size, PDI, zeta potential and EE were performed over a period of 12 weeks using the two previously described procedures, DLS and UV-vis spectroscopy respectively. All this stability tests were made in triplicate in order to reach statistical significance. During the period of the study nanoformulations were kept at 4°C.

2.6 Cellular studies

2.6.1 Hemolysis assay

The most frequently test used to initialize *in vitro* tests is the hemolysis assay. This study was carried out to assess the SLN's hemolytic potential by monitoring the release of hemoglobin, a marker of RBC lysis in response to drug/NP exposure [106].

To perform this assay, human blood samples from three distinct donors were kindly donated by Serviço de Hematologia from Centro Hospitalar Universitário do Porto - Hospital de Santo António. (Porto, Portugal). Prior to use, blood samples were collected into tubes containing the anticoagulant EDTA. The plasma fraction (supernatant) that resulted from centrifuging blood samples at $955 \times g$ for 5 min at $4^{\circ}C$ was taken out of the sample. After that, the pellets containing the red blood cells (RBC) were washed three times with physiological sterile saline solution (0.85% w/v). The last washing phase was followed by dilution in saline solution, to obtain an RBC concentration of 4% (v/v).

The nanoformulations were then diluted in saline solution, with final concentrations ranging from 2 to 32 μ M of VP. Triton-X-100 at a concentration of 1% (v/v) and saline solution (0.85%) were chosen as the experiment's positive and negative controls, respectively [107].

Each sample was added in triplicate into a 96-well microplate (Kartell, Noviglio, Italy) for the test. Following the addition of 100 μ L of either sample or control to the wells, 100 μ L of RBCs were then added to each well to produce the final concentrations. The plate was then incubated at 37°C for 1h. After that, microplates were centrifuged at 955 x g for 5 min and 100 μ L of the supernatant were carefully pipetted to a clear 96-well plate to measure the amount of released hemoglobin by determining the absorbance at 540 nm (Biotek Instruments, Winooski, VT, USA).

For the calculation of the percentage of hemolysis, control wells with 100 μL of each nanoformulation concentration in saline solution without red blood cells were prepared for background subtraction.

The percentage of hemolysis was calculated as follows:

(Equation 5)

$$Hemolysis \% = \frac{Abs \, (sample) - Abs \, (negative \, control)}{Abs \, (positive \, control) - Abs \, (negative \, control)} \times 100$$

2.6.2 Cell culture

MCF-7 and L929 cells were cultured at 37°C in a 5% CO2 atmosphere (Unitherm CO2 Incubator 3503 Uniequip; Planegg, Germany) in Dulbecco's Modified Eagle Medium (DMEM) supplemented with 10% Fetal Bovine Serum (FBS) 1% Penicillin- Streptomycin (Pen-Strep). Cells were rinsed twice with DPBS and new supplemented DMEM was added to the medium every two to three days. When cell confluence reach about 80 to 90%, cells were chemically detached with 0.25% trypsin-EDTA, centrifuged at 300 g for 5 min (Multifuge X1R, Thermo Fisher Scientific, USA), and then re-suspended in new media. Cells were seeded at a density of 750000 cells per 75 cm2 flask (Tissue Culture flasks, Orange Scientific, Belgium) in complete DMEM (10 mL). Cell counting was carried out by diluting cells at a ratio of 1:10 in Trypan Blue solution (0.4% (w/v) in PBS), as a way to exclude non-viable cells, using a Neubauer chamber (Improved Neubauer Bright-line, Boeco; Germany).

2.6.3 Cellular uptake visualization using Confocal laser scanning microscopy

In the past few decades, the CLSM technique has gained popularity in the fields of biology, biomedicine, and material sciences. Contrary to typical optical microscopes, confocal microscopes use a spatial pinhole in front of a detector to focus the light on a certain depth and filter out any information outside of the focal plane. In CSLM, optical sectioning is made possible by the depth-selective laser beam used as the light source. To ensure that only the light from the little region of the sample that is exposed to radiation is detected, the information obtained from this focal point is projected onto a pinhole in front of the detector. By comparing the pictures produced by conventional optical microscopy and CLSM in reflected light mode has demonstrated the higher resolution and hence the superior quality of the images obtained with CLSM. Finally, a CLSM scans the surface point by point to build the image. The major advantage of CLSM over other microscopy methods is the ability to reconstruct 2D images into 3D representations by performing this in the x-y plane for various depths in z-direction [108].

NPs and Free VP internalization into MCF-7 cells was observed using CLSM. MCF-7 cells were cultured in supplemented DMEM at 37° C, 5% CO2 and seeded at a density of $1x10^{4}$ cells per well in 8 well- μ -slides (Ibitreat, Ibidi GmbH, Munich, Germany). Cells were cultured

with free VP, functionalized and non-functionalized VP-loaded SLN (0.125 μ M VP) for 3 h at 37°C and 5% CO₂ after 24 h. After washing with PBS three times, the cells were fixed with formalin solution for 30 min at room temperature. After another three-strep washing with PBS, cells were stained with Hoechst (8 μ M in PBS) to mark the cell nucleus and let to sit at room temperature in the dark for 10 min followed by washing three times with PBS. Images of internalization of the NPs and free VP into MCF-7 cells were acquired on a Leica Stellaris 8 confocal microscope (LeicaMicrosystems, Wetzlar, Germany) equipped with the Leica Application Suite X package (LAS X) using a λ ex/ λ em of 350/461 nm (Hoechst 33342®) and λ ex/ λ em of 650nm/690 (VP) with a resolution of 1024 × 1024 using a 63X/1.4 oil immersion objective. CLSM studies were performed at the Imaging by confocal and fluorescence lifetime laboratory, CEMUP, Portugal.

2.6.4 Cell viability assay

Cell viability can be assessed using different methodologies, including the Resazurin assay, a fluorescent assay that can monitor cellular metabolic activity for up to 24-48 h. The rationale behind this technique relies on the capacity of metabolically active cells to convert the blue, non-fluorescent reagent resazurin into the highly fluorescent reagent resorufin. As a result, the amount of resorufin generated and its fluorescence are directly related to the number of metabolically active cells present in the sample. The amount of resorufin generated is measured using a fluorometer using relative fluorescence units (RFU) [109, 110].

L929 and MCF-7 cell viability following incubation with the produced nanoformulations was measured by performing a resazurin assay.

First, 1x10⁴ MCF-7 and L929 cells were seeded onto 96-well tissue culture plates (Falcon®, Becton Dickson; England) and incubated for 24 h at 37 °C, 5% CO2. The SLN-VP, SLN-VP-FA, and free-VP formulations were then diluted in DMEM to provide the following VP concentrations: 0.5, 1, 5, 10, 20, 30, 50 μ M (for the initial assay and determination of the drug IC50) and 0.125, 0.250, 0.5, 1, and 2 μ M (for the following studies). After this, cells were exposed to 100 μ L of each concentration of the two formulations and free VP, and they were then incubated for 24 h at 37 °C and 5% CO2. A positive control containing cells treated with only DMEM was also included. Additionally, to account for background fluorescence, a control that contained only resazurin (and no cells) was also added. After 24h of incubation 110 μ L of resazurin (10%v/v in DMEM) were added to each well. After 2h of incubation in the dark, the supernatant was transferred to a black-well clear bottom 96 well plate and the fluorometer (Biotek Instruments, Winooski, VT, USA) (λ ex = 560 nm; λ em = 590 nm) was used to measure the fluorescence of resorufin.

Cell viability was calculated using the following equation:

(Equation 6)

$$\textit{Cell viability (\%)} = \frac{\textit{Fluorescence of sample} - \textit{Fluorescence of resazurin}}{\textit{Fluorescence of positive control} - \textit{Fluorescence of resazurin}} \times 100$$

For the light-irradiation experiments, MCF-7 cells were seeded at a density of 1x10⁴ cells per well and incubated for 24h, After that, the different nanoformulation or free VP were added to the cells and incubated for 3h followed by irradiation with a LS-LED LED Light Source (LED slide of 690 nm) coupled to a Vis/NIR Optical fiber (50cm, 600µm core diameter, Sarspec, Porto, Portugal), at 0.57, 2.15 or 4.16 mW for 2, 5 or 10 min for the initial studies, and 2.15 mW and 5 min for the following PDT studies. The resazurin assay was then carried out on the following day as described before. The light fluence was estimated using the following equation (taking into account that the light spot had an area of 0.32cm²):

$$Fluence(J/cm^2) = \frac{Laser\ Power(W) \times Irradiation\ period(s)}{Well\ area(cm^2)}$$

2.6.5 ROS quantification assay using Flow cytometry

The main principle of flow cytometry is the single-file passage of cells in front of a laser for detection, counting, and classification. Fluorescently marked cell parts are activated by the laser and emit light at various wavelengths [111].

When cells are exposed to a light source one at a time, they scatter light, which is used by flow cytometry, a multiparameter technique, which can separate cells using three direct signals: forward scatter, side scatter and fluorescence. The cell volume can be determined by the forward scatter's amplitude. The side scatter reveals details about the components of the cell, such as the nuclei and granules. Fluorescence can be used to quantify any fluorescence marker of molecule within the cell. The structural and functional cell characteristics are associated with these signals. Contrary to other biochemical methods, which often provide the average of a high number of cells, flow cytometry enables the investigation of a range of organisms or particles, including complete cells, chromosomes, organelles, or protoplasts. These measures are acquired at a sample rate of thousands of particles per second [111].

Flow cytometry can be used to perform numerous cell-based assays, including the quantification of ROS production. The fluorescence methodology relies on the use of appropriate probes to assess ROS production into the cells. 2',7'-dichlorofluorescin diacetate (DCFDA) is a fluorometric probe for the detection of H2O2 and one of the most common probes than can be used to estimate ROS production. DCFDA is also a non-fluorescent,

lipophilic, and non-ionic substance that as the ability to diffuse and cross cell membranes into the cytoplasm. After entering into the cell, DCFDA is deacetylated by intracellular esterases, resulting in the formation of 2',7'-dichlorofluorescin (DCFH), a non-fluorescent molecule that is membrane impermeable and interacts with intracellular ROS [112]. DCFH can then be converted into the fluorescent 2', 7'-dichlorofluorescein in the presence of ROS (DCF). The amount of DCF fluorescence is proportional to ROS activity and can be measured by spectrofluorometry, flow cytometry of confocal microscopy. Most often, a single measurement of the emitted fluorescence at a single chosen time-point is made, and the result is used as a qualitative indicator of cellular oxidative stress [112]. This quantification is a very important assay in PDT because it is related to the mechanism of action of the PS, being the mechanism by which cancer cells are killed.

The production ROS in MCF-7 cells induced by the nanoformulations and free VP with and without light irradiation was quantified by flow cytometry using the DCFDA probe. Briefly, MCF-7 cells were seeded into 96-well plates at a density of 3x10⁴ cells per well and cultured for 24 h. Subsequently, the different VP-loaded SLN and free VP at a concentration of 0.25 μM of VP were added to the cells. For the light irradiation samples, after 3h of incubation, cells were illuminated with a LS-LED LED Light Source (LED slide of 690 nm) at 2.15mW for 5 min (2 J/cm²) to activate the PS VP and elicit the production of ROS. After that, media was removed and cells were incubated with DCFDA (10 μM in PBS) for 30 min in the dark at 37°C. Cells were then washed twice with PBS, detached with trypsin-EDTA 0.25% (w/v), centrifuged for 5 min at 300g, and resuspended in PBS. A BD Accuri TM C6 flow cytometer (BD Biosciences, Erembodegem, Belgium) was used to measure ROS, and at least 10,000 events were collected for each sample. Data were examined (BD Biosciences, Belgium) using the BD AccuriTM C6 software.

2.6.6 Apoptosis induction assessed by flow cytometry

Annexin V, also known as annexin A5, is a member of the annexin family of intracellular proteins which interacts with phosphatidylserine in a calcium-dependent manner. In normal healthy conditions, phosphatidylserine is exclusively located on the intracellular leaflet of the plasma membrane, however, when a cell enters early apoptosis, the membrane's asymmetry is disrupted, and phosphatidylserine translocates to the external leaflet. Annexin V that has been fluorescently labeled with Fluorescein isothiocyanate (FITC) can then be utilized to target and distinguish apoptotic and living cells. Since annexin V binding cannot distinguish between necrotic and apoptotic cells, the combined use of 7-amino-actinomycin D (7-AAD) solution can give more information in this regard. Due to the passage of these dyes into the nucleus, where they bind to DNA, early apoptotic cells will exclude 7-AAD, whereas late stage apoptotic cells will stain positively [113].

According to the manufacturer's instructions, the FITC Annexin V Apoptosis Detection Kit with 7-AAD (Biolegend®, California, USA) was used to measure the amount of apoptosis that the nanoformulations and Free VP caused in MCF-7 cells with and without light irradiation. Briefly, MCF-7 cell were seeded in 96-well plates at a density of 3x104 cells per well and cultured for 24 h with supplemented DMEM. Cells were then treated with the various nanoformulations and Free VP at 0.125 μM. For the light-irradiation experiments, after incubation with the nanoformulations for 3h, cells were illuminated with a LS-LED LED Light Source (LED slide of 690 nm) at 2.15mW for 5 min or (2 J/cm2). Following 24 h, cells were detached using trypsin-EDTA 0.25% (w/v), centrifuged for 5 min at 300g, and washed twice with cold PBS. The cells were then resuspended in Annexin V binding buffer, stained with FITC Annexin V and 7-AAD according to the manufacturer's instructions, and incubated at room temperature for 15 min in the dark. A BD Accuri C6 flow cytometer (BD Biosciences, Erembodegem, Belgium) was used to measure apoptosis, and at least 10,000 events were collected for each sample. Data were examined (BD Biosciences, Belgium) using the BD AccuriTM C6 software.

2.6.7 Statistical analysis

Statistical analysis was performed using Graphpad Prism9 Software (GraphPad Software Inc., San Diego, CA, USA). Data were analyzed using one-way analysis of variance (ANOVA) with Tukey's multiple comparisons test or two-way ANOVA using Tukey's test with a p-value < 0.05 considered statistically significant. Data are expressed as mean \pm SD.

3 Chapter Results and Discussion

3.1 Production of Verteporfin-loaded solid lipid nanoparticles

The nanoformulations were produced using specific amounts of lipids and a specific production protocol that was established in a previous work [95]. After 2 weeks, a preliminary stability test was conducted to evaluate if the NPs remained stable. Subsequently, a DSPE-PEG2000-FA conjugate was synthesized and functionalized SLN were produced by adding the conjugate (PEG2000-FA) to the lipid phase, at a ratio of 1% w/w of the total lipid mass. After 2 weeks both functionalized and non-functionalized SLN showed stable size, PDI, zeta potential and EE%.

After a preliminary experiment to establish the ideal amounts of solid lipid, surfactant and VP to maximize the EE and maintain the nanoformulations within a range of sizes suitable for intravenous administration (≈200 nm), 3 different formulations were produced in triplicate: the functionalized unloaded SLN (SLN-FA), non-functionalized VP-loaded SLN (SLN-VP) and functionalized VP-loaded SLN (SLN-FA-VP). The obtained VP-loaded formulations presented a homogeneous dark green color, contrasting to the milky white appearance of the unloaded formulations. All of the nanoformulations remained homogeneous with absence of precipitates during the period of the study.

The properties of the different nanoformulations prepared were compared to assess the influence of VP loading and DSPE-PEG-FA functionalization on the NPs main physicochemical characteristics and to evaluate if the NPs have adequate characteristics for the desired purpose.

3.2 Physicochemical characterization

The produced nanoformulations were characterized in terms of size, PDI, zeta potential, EE and LC as shown in Table 2. As the work is intended for intravenous administration for a subsequent tumor passive accumulation, it can be said that the sizes obtained ranging from 190 to 249 nm are suitable for that purpose [114-116]. PDI remained at values below 0.2, suggesting that a homogenous population of NPs was obtained and it was also evident that the size of the NPs was not greatly impacted by the functionalization [117].

Zeta potential was in the range of -25 mV for all the nanoformulations produced, meaning that the NPs have a high stability in suspension, with a limited aggregation tendency due to the repulsion forces induced by this highly negative surface charge [118]. No statistically significant differences were found in this parameter for all the formulations, suggesting that the surface functionalization and VP loading did not affect the particles stability. Very high

values of EE were obtained for both functionalized and non-functionalized SLN, which suggests that the developed SLN are suitable nanocarriers for VP.

Table 2 - Physicochemical characterization of the final formulations: size, PDI, zeta Potential, EE and LC.

	SLN-FA	SLN-VP	SLN-FA-VP
Size (nm)	223 ± 4	193 ± 8	225 ± 3
PDI	0.15 ± 0.01	0.16 ± 0.02	0.18 ± 0.05
Zeta Potencial (mV)	-25 ± 5	-28 ± 7	-24 ± 2
EE (%)	N/A	98 ± 3	97 ± 3
LC (%)	N/A	2.34 ± 0.06	2.30 ± 0.06

3.3 Stability studies

To evaluate the physical stability of the nanoformulations the particle size, PDI, zeta potential and EE were evaluated regularly over a period of 12 weeks after storage at 4°C.

The stability of size and PDI over the 12 weeks is shown in Figure 6. On A and B, all 3 SLN show small variances in terms of size and PDI, with only significant different values found in week 8. Nevertheless, after 12 weeks, no statistically significant differences compared to the week 0 were observed. For all of the time points studied particle size remained adequate for intravenous administration and the values of PDI were maintained around the 0.2 value, which is an acceptable value for lipid-based NPs, suggesting the presence of an homogeneous NP population [117].

In terms of zeta potential (Figure 6C), there were no significant alterations during the 12 weeks period of the study, which suggest that the NPs remained stable and did not aggregate during this period.

To evaluate the eventual release of VP of the NPs over time, the EE was also measured periodically. As demonstrated in Figure 6D, there were no statistically significant differences during the 12 weeks of the study with a value of EE obtained remaining higher than 95% . This highlights the high stability of the nanoformulations for at least 12 weeks. Overall, the stability study performed demonstrates that the nanoformulations produced are stable for at least 12 weeks.

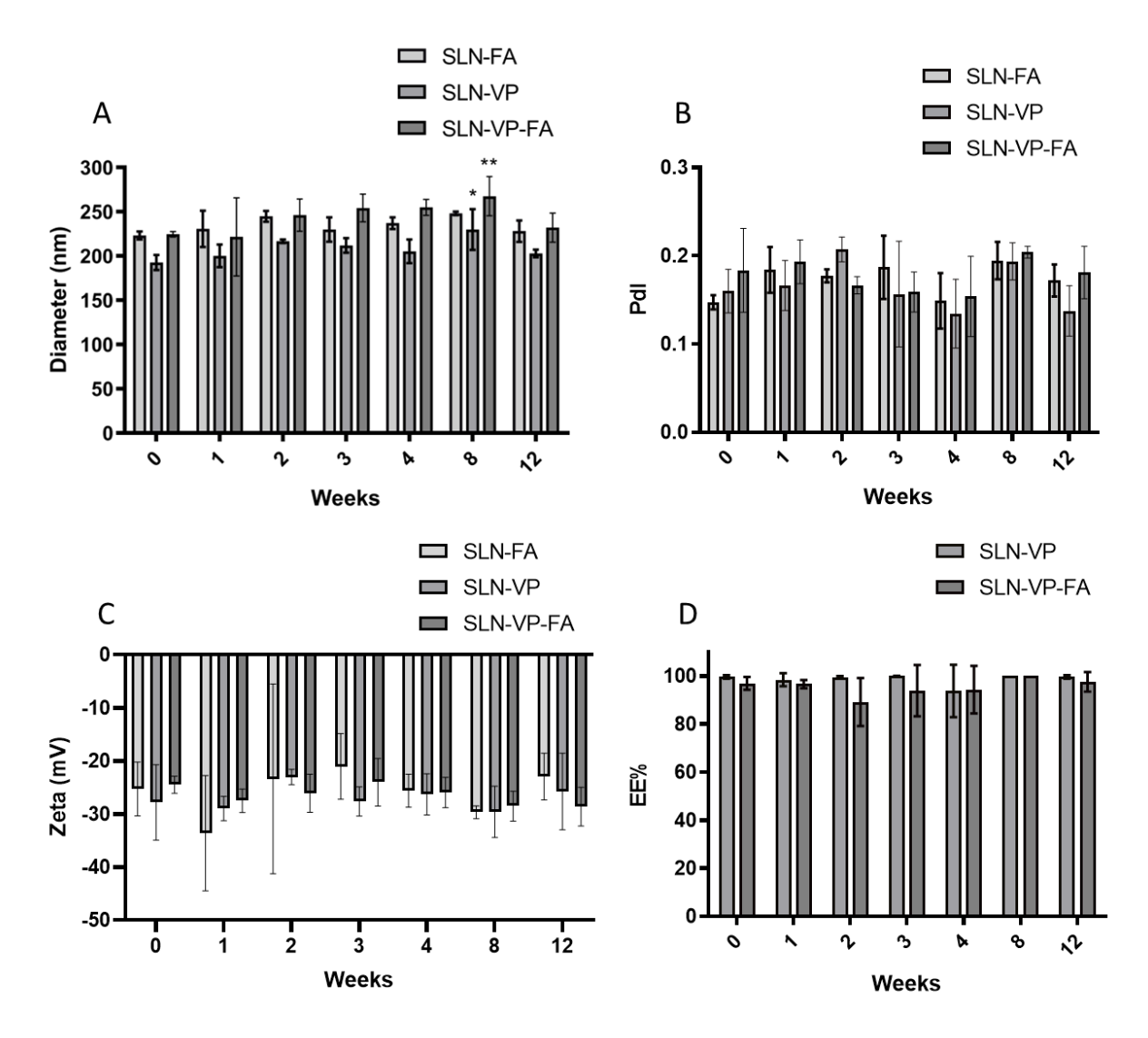


Figure 6- Effect of time of storage on (A) size. (B) PDI of the nanoformulations. (C) Effect of time of storage on zeta potential of VP-loaded nanoformulations functionalized and nonfunctionalized with DSPE.PEG-FA conjugate. (D) Effect of time of storage on EE of VP-loaded nanoformulations functionalized and nonfunctionalized with DSPE.PEG-FA conjugate. Values represent the mean \pm SD (n=3), *p<0.05, **p<0.01. All statistically significant differences are related to the values of the correspondent nanoparticles at week 0. Differences between groups were determined using two-way ANOVA followed by Dunnett's multiple comparations test.

3.4 Cellular studies

3.4.1 Hemolytic effect of the nanoformulations

The hemolytic potential of the SLN in concentrations ranging from 2 to 32 mg/mL of lipid after incubation for 1h is shown in Figure 7. The RBC toxicity of SLN loaded with VP was assessed *in vitro* at the same conditions previously described in the materials and methods section. As seen in the graph, the hemolytic activity was not higher than 0.03% for all of the nanoformulations at the range of concentrations tested (Figure 7). Taking into account that all the values were below the 5% hemolysis reference value, the nanoformulations are considered

non-toxic and therefore safe and suitable to be administered intravenously, according to ISO 10993-4 [119]. Therefore, these data supports that the developed nanoformulations are not hazardous as drug carriers administered intravenously [119].

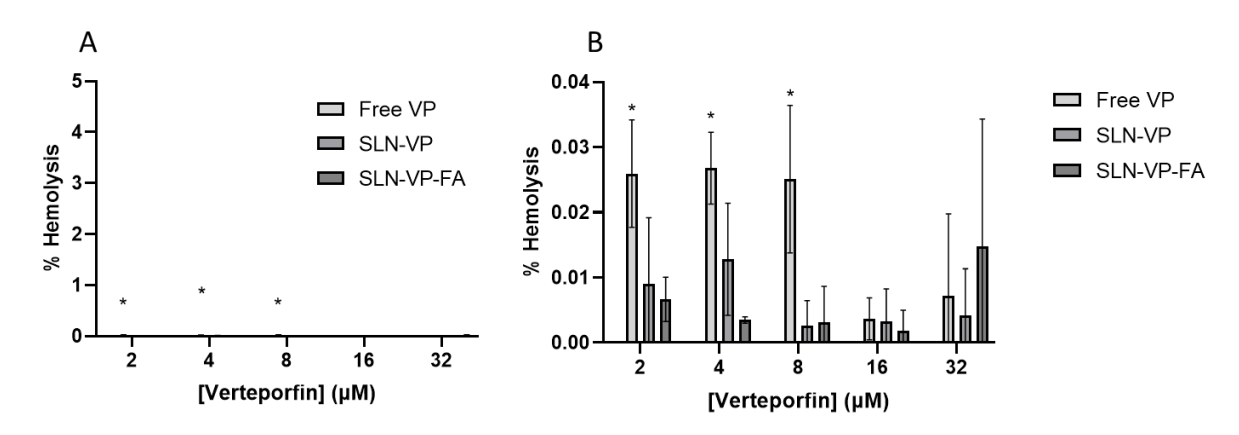


Figure 7 - (A) In vitro hemolysis assay results for diluted human blood exposed to different concentrations (2, 4, 8, 16, 32 (μ M) of Free VP and VP-loaded formulations. (B) is an amplified view of (A). Values represent mean \pm SD (n=3)), (*) denotes statistically significant differences relatively to the correspondent Free VP 16 μ M (P<0.05). Differences between groups were determined using two-way ANOVA followed by Tukey's multiple comparations test.

3.4.2 Nanoparticle uptake into MCF-7 cells visualized by Confocal microscopy

To study the uptake of the NPs and get some insights on the efficacy of the active targeting strategy, confocal microscopy was used for the visualization of MCF-7 cells following incubation with free VP, functionalized and non-functionalized SLN for 3 h. As presented in Figure 8, after the 3h incubation, both VP-loaded SLN and Free VP have been internalized by MCF-7 cells, being mostly located in the cytoplasm region as seen by the red fluorescence signal. This suggests that both SLN are able to effectively deliver VP to the cytoplasm of the cell. As expected, no red signal was observed for the control group. The overall results demonstrate that SLN could deliver VP to MCF-7 cells after 3h incubation, suggesting that these incubation time-point may be explored for subsequent PDT experiments.

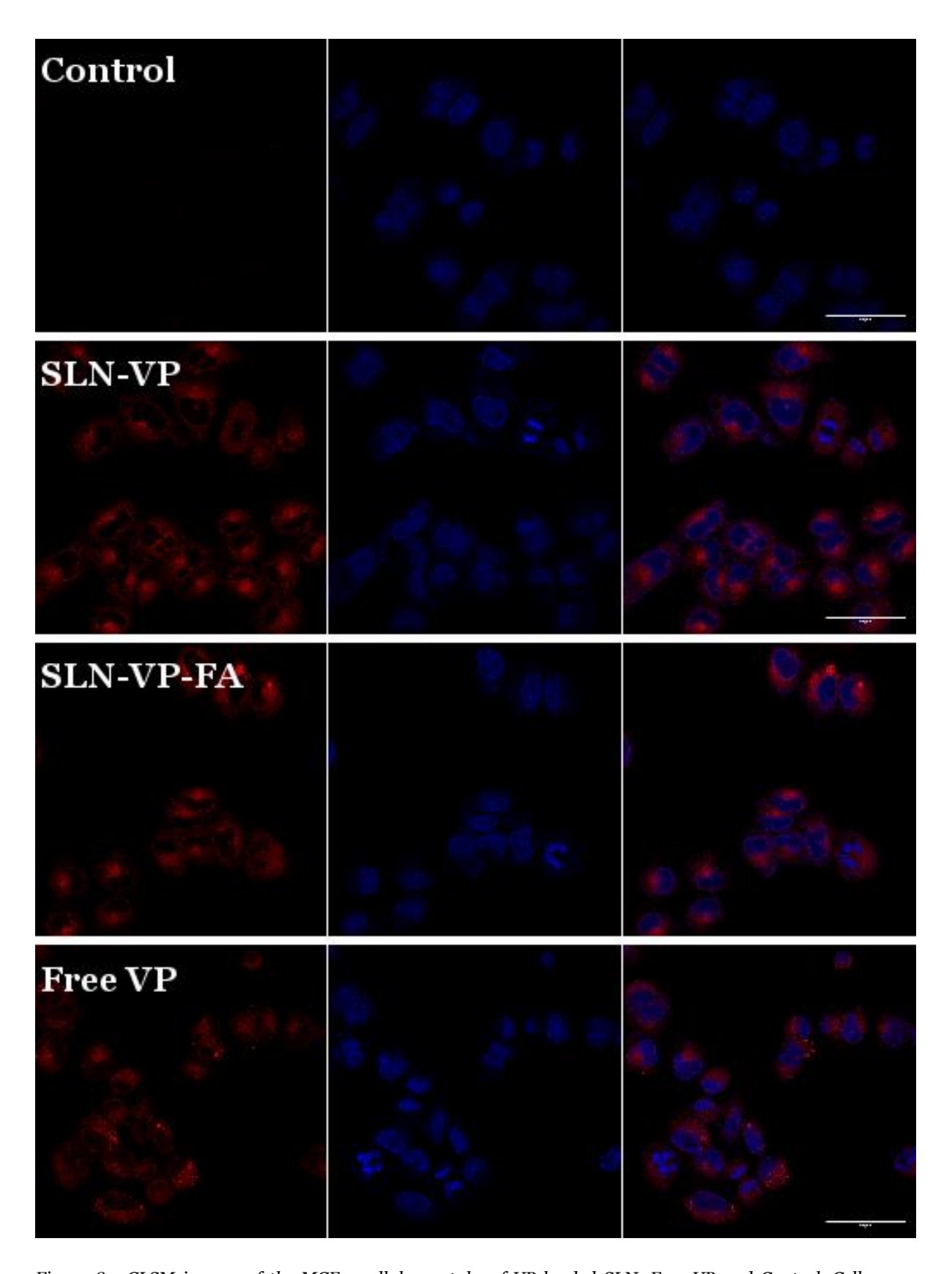


Figure 8 - CLSM images of the MCF-7 cellular uptake of VP loaded SLN, Free VP and Control. Cells were incubated with the nanoformulations for 3 h. Blue channel: Hoechst 33342 (nucleus). Red channel: VP

3.5 In vitro photodynamic therapy studies

3.5.1 Free Verteporfin dark cytotoxicity: preliminary assay

To gather information regarding the toxicity of the free VP and establish the range of concentrations to be used in future studies a preliminary assay of the toxicity of free VP in dark conditions in MCF-7 cells was performed using the resazurin assay. To obtain the results of IC₅₀ the assay was done from concentrations ranging from 0.5 to 50 μ M and the cell viability was then assessed for each condition. An IC₅₀ of 15.36 μ M of Free VP (Figure 9) was obtained, meaning from at this concentration and upwards it is expected to obtain less than 50% cell viability, which is are not the most suitable results for an ideal dark toxicity of VP. However, this IC₅₀ value is relatively high leaving room to assess the PDT of VP using lower concentrations of VP, in which the cell remained viable as some research show IC₅₀ with irradiation of 0.21 μ M [120].

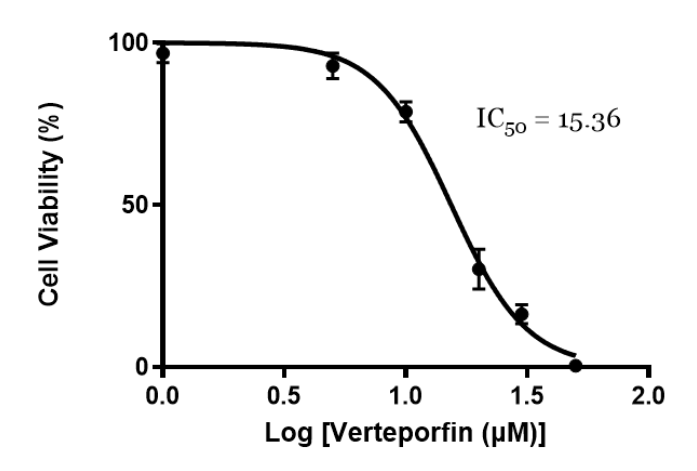


Figure 9 - Dose-response curves of MCF-7 cells incubation with free VP for 24h.

3.5.2 SLN dark cytotoxicity assessment in normal (L929) and cancer (MCF-7) cells

After establishing the safe concentrations of VP, the cytotoxicity induced by VP-loaded NPs was evaluated in both L929 normal cells and MCF-7 breast cancer cell line using the Resazurin assay. The MCF-7 cell line was chosen as a reference cancer cell line and also due to its overexpression of the folate receptor. The L929 fibroblast cell line was also used as a normal cell line model and since it is recommended by the ISO international standard 10993–5 for biocompatibility assessment studies [121].

After incubation of the cells with NPs for 24h, the cell viability was calculated as being directly proportional to the amount of resorufin fluorescence produced by metabolically active cells. As shown in Figure 10, functionalized and non-functionalized nanoformulations were non-toxic (<70%) up to a concentration of VP (2 μ M) according to ISO 10993-5 [121]. No statistically significant differences were observed in terms of cell viability reduction caused by functionalization of SLN. This suggests that VP before being photoexcited does not produce toxicity to both tumoral (A) and normal (B) cells at the range of concentrations tested. However, it is noticed a slight lower viability after treatment with Free VP compared to the NPs in the L929 (B), suggesting that SLN can protect the cells from some of the intrinsic toxicity of the free VP.

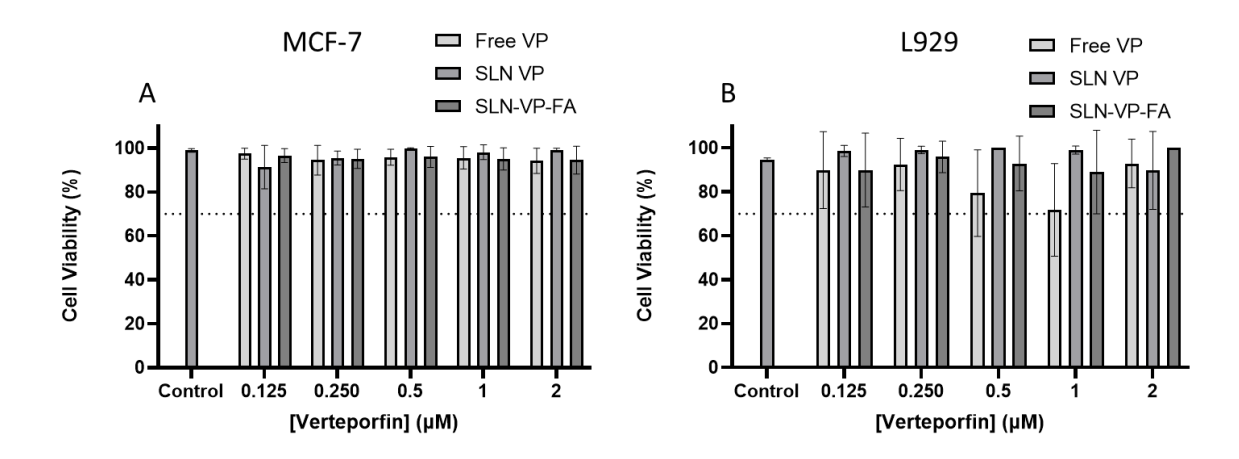


Figure 10 - MCF-7 cell viability assessed by the Resazurin assay after 24 h of exposure to the different nanoformulations and free VP at increasing concentrations of SLN, representing the dark toxicity of the nanoformulations and free VP. Values represent the mean \pm SD (n>3).

3.5.3 Cancer cell cytotoxicity upon light irradiation: parameters optimization

In this work, a LED light source with a 690 nm LED slide, was used, attached to an optical fiber to have a better and more precise irradiation of the MCF-7 cells. At first, to optimize the results to the best possible extent, different irradiation times and different irradiation intensities were tested. Three different irradiation times were evaluated: 10min, 5min and 2min, as showed in figure 11A, and three different intensities were tested: a high, medium and a low irradiation intensity, corresponding to 3.9 J/cm², 2 J/cm² and 0.5 J/cm², respectively (Figure 11B). All of these optimization assays were done using only free VP. The time test (A) was made at high intensity (3.9 J/cm²) and the Intensity test (B) was made at 5 min irradiation time. By analyzing the time test (Figure 11) it was possible to conclude that the 5 and 10 min irradiation times were quite similar in terms of cancer cell death. Therefore, 5 min of irradiation was selected to proceed with further studies. In the case of the intensity test it was observed that medium intensity irradiation resulted into similar outcomes to the ones

obtained following exposure to high intensities. Therefore, irradiation with medium intensity (2 J/cm^2) was selected for the following studies. Importantly, it was also demonstrated for all the conditions tested that light irradiation by itself (control group) does not result in a higher cancer cell mortality, demonstrating the safety of the light source used.

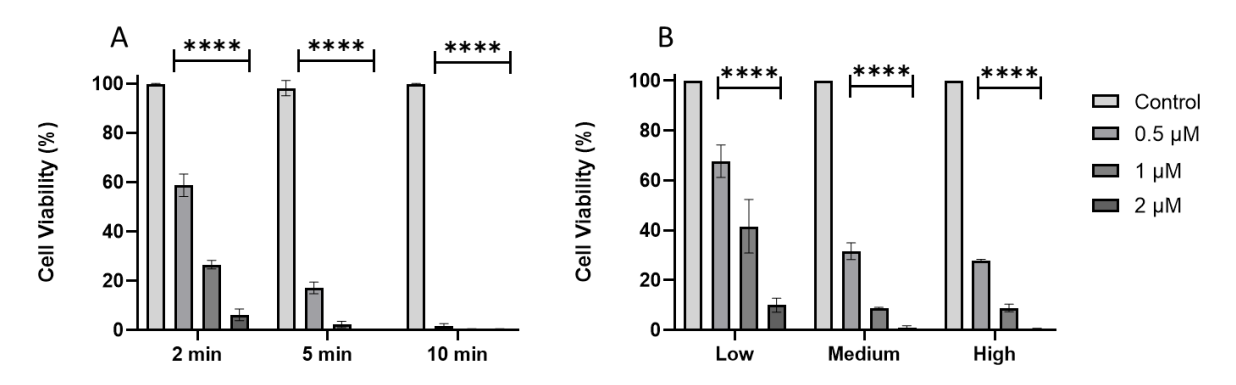


Figure 11 - MCF-7 cell viability assessed by Resazurin assay after 24 h of exposure to the different times (A) and different intensities (B), not exposed to light. Values represent the mean \pm SD (n>3) (****) denotes statistically significant differences of p<0.0001 relatively to the correspondent Control. Differences between groups were determined using two-way ANOVA followed by Dunnett's multiple comparations test.

3.5.4 Assessment of the Photodynamic therapeutic effect in MCF-7 cells

The aim of this assay, which is one of the most important tests done throughout the whole study, is to prove that VP and VP-loaded SLN can effectively induce cancer cell death upon light irradiation, demonstrating the occurrence of PDT.

In the previous section VP was found to be non-toxic to both normal and cancer cells in dark conditions (without the occurrence of PDT). In this assay, after a previous 3h incubation of free VP, SLN VP and SLN-VP-FA at the same range of concentrations tested in dark conditions, the LS-LED + fiber optic were employed to irradiate the MCF-7 cells using the previously optimized conditions of medium intensity (2 J/cm²) and 5 min duration. After 24 h, the resazurin assay was carried out and the obtained results of cell viability are highlighted in Figure 12.

As presented in Figure 12, a dose-dependent cytotoxicity was obtained for all the nanoformulations and free VP, promoting a decrease of more than 50% in cell viability with doses of 0.5 μ M or higher for the nanoformulations. For Free VP, a dose of 0.25 μ M was enough to promote a decrease of more than 50% in cell viability, which in consistent with the literature, where Free VP IC50 was below 0.25 μ M after light irradiation [120]. This is a much lower concentration needed compared with the 13.56 μ M obtained for the dark toxicity studies previously described. This result suggests that the mechanism of action of VP as a PS is maintained even when incorporated into SLN.

Another important aspect is the fact that Free VP promotes a higher decrease in cell viability comparing to the corresponding functionalized and non-functionalized SLN. This suggests that VP has a high anti-tumoral activity upon light irradiation as seen by the

reduction of cell viability (to 40%) after incubation with the lowest concentration tested (0.125 μ M). This suggests that when incorporated into SLN the anti-tumoral effects of VP is less accentuated, which can be related to a time-dependent release of VP from the SLN, which makes its effects less immediate than the free VP. Additionally, SLN may enter into the cells at a lower rate than the free VP, due to different cellular entry mechanisms. Nevertheless, after treatment with higher concentrations, SLN ended up inducing high anti-tumoral effects, as desired. For instance, at 2μ M (which is a low concentration with a low dark toxicity) the cell viability is less than 5% for all of the conditions tested following light irradiation. Moreover, the use of SLN can improve the solubility of VP, limit its off-targeted systemic distribution and improve its accumulation in the tumor region. Therefore, by incorporating VP into SLN, lower drug dosages may be needed to induce similar anti-tumoral effects.

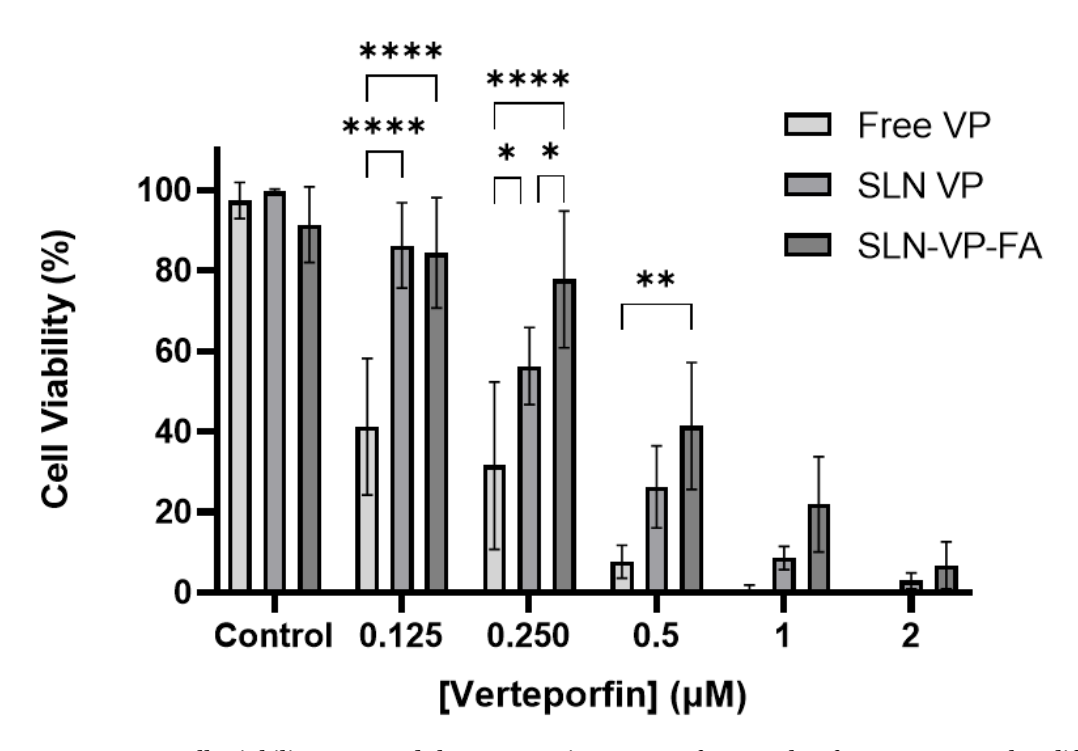


Figure 12 - MCF-7 cell viability assessed by Resazurin assay after 24 h of exposure to the different nanoformulations and free VP at increasing concentrations of SLN, exposed to light (PDT treatment). Values represent the mean \pm SD (n>3). *p<0.05, **p<0.01, ****p<0.001 denotes statistically significant differences. Differences between groups were determined using two-way ANOVA followed by Tukey's multiple comparations test.

3.5.5 Induction of apoptosis under dark and light conditions in MCF-7 cells

The triggering of apoptosis induced by each nanoformulation, and free VP was studied using FITC Annexin V Apoptosis assay with 7-AAD. VP is having been shown to regulate the expression of proteins involved in cell cycle progression and apoptosis by disrupting the YAP-TEAD interaction in breast cancer cells [122]. Additionally, apoptosis is one of the mechanisms by which PDT exerts its effects, as described in the introduction section. Therefore, in this assay, the ability of free VP and the different nanoformulations to induce apoptosis in MCF-7 cells with (Figure 11 A) and without (Figure 12 B) light irradiation was evaluated following incubation at a concentration of 0.125 µM of VP. At dark conditions (Figure 13 A), the percentage of viable cells obtained was 97% for all cases, which corroborates the cell viability assays at this concentration, suggesting a low dark toxicity for all of the conditions tested. In contrast, in the assay of PDT (Figure 13B) a higher level of apoptosis occurred following incubation with SLN-VP, SLN-FA-VP and free VP, comparing to the control. Early apoptosis was almost at 15% for each SLN treatment and 40% for the Free VP, which were higher than the 3% of apoptosis from the control group. Late apoptosis events were only observed after treatment with free VP with 6% of cells in late apoptosis. These results are consistent with the cancer cell toxicity assays presented in the previous section for this concentration, where the free VP was found to exert more immediate PDT effects. This suggests once more that the nanoformulations have less immediate anti-cancer effects than the free VP but, on the other hand, can maintain the apoptotic effects and the PDT mechanism of action of the drug. Overall, the apoptosis assay demonstrates that VP is more controlled in its apoptotic effects towards MCF-7 cells after incorporation into SLN. Nevertheless, the existence of PDT is confirmed, with clear differences in apoptosis induction between dark and light irradiated samples.

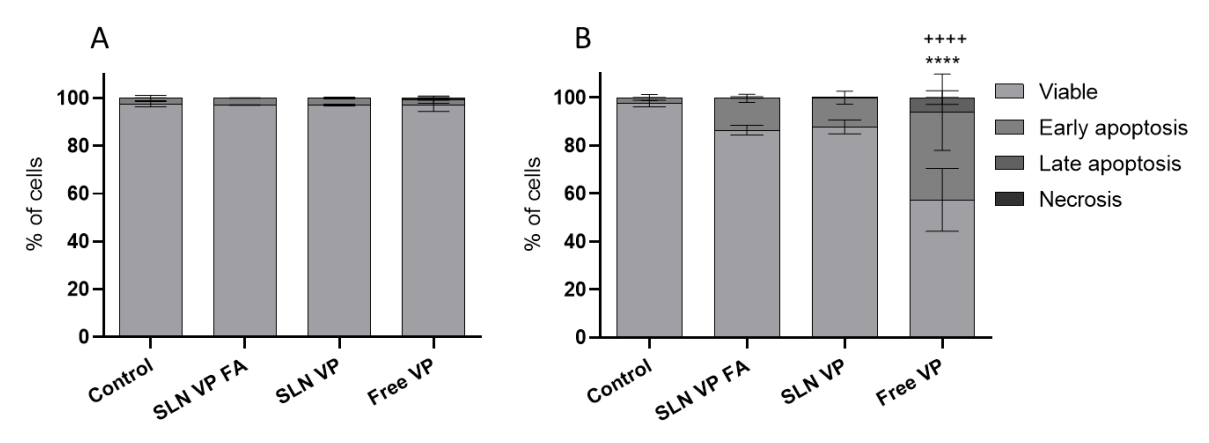


Figure 13 - Apoptosis of MCF-7 cells following incubation with the nanoformulations at a concentration of 0.125 μ M of VP using the FITC Annexin V Apoptosis assay. Data expressed as mean \pm SD (n = 2). All statistically significant differences are the differences between each treatment and control group: Viable: **** p < 0.0001; early apoptosis: ++++ p < 0.0001. Differences between groups were determined using two-way ANOVA followed by Dunnett's multiple comparations test.

3.5.6 Production of reactive oxygen species upon light irradiation in MCF-7 cells

To evaluate the production of ROS upon light irradiation, a quantitative analysis was performed by flow cytometry using 2',7'-Dichlorofluorescein diacetate (DCFDA). DCFDA is a cell-permeable non-fluorescent probe which is de-esterified intracellularly and turns to a highly fluorescent compound upon oxidation, DCF [112]. Applications include sensitive and rapid quantitation of oxygen-reactive species in response to oxidative metabolism caused by the PDT treatment. The mean fluorescence measured within the cells with and without light irradiation after incubation with the NPs is shown in Figure 15.

It is possible to observe a limited amount of ROS production in dark conditions for all the treatments, once again demonstrating that this PS does not produce ROS by itself. On the other hand, significantly higher levels of ROS were observed after light irradiation. In fact, approximately 2-times higher fluorescence was observed for SLN-VP-FA and 3-times for Free VP when compared with their respective assay with no light. Moreover, it was also demonstrated that the light irradiation by itself did not induce significant levels of ROS production, as it can be observed in the control group. These encouraging results are in agreement with the results of the cell viability and apoptosis assays obtained earlier, suggesting a direct correlation between ROS formation and reduction of cancer cell viability.

These findings can also be observed in figure 15 obtained with confocal microscopy, suggesting that there is a high green signal of the DCF molecule when subjected to light irradiation.

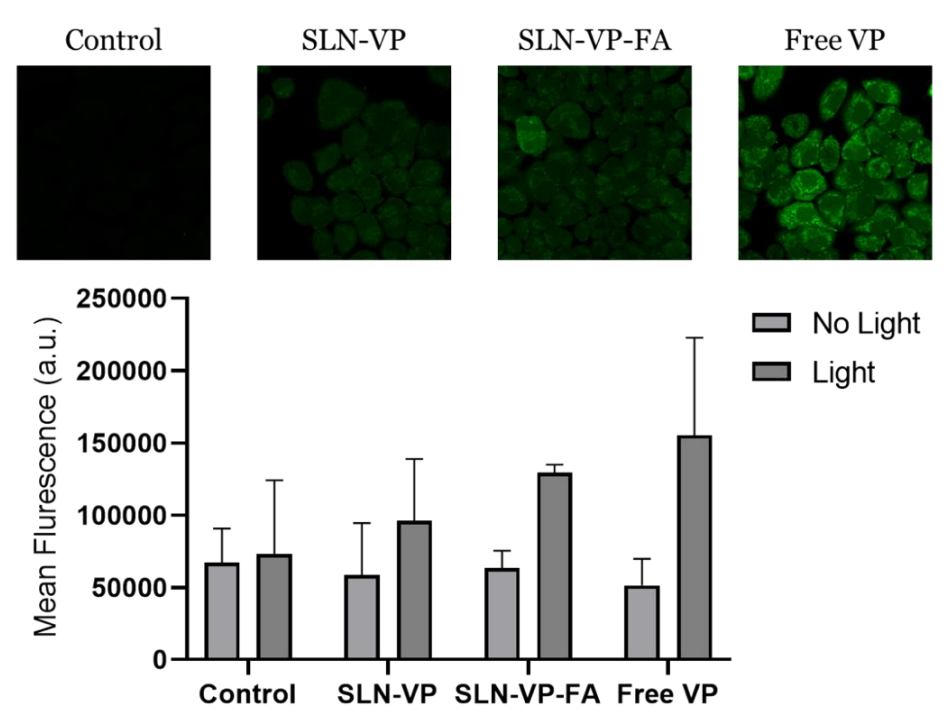


Figure 14 - Quantification of MCF-7 cellular uptake of VP-loaded SLN and Free VP by flow cytometry. Cells were incubated for 3h with an equivalent concentration of 0.25 μ M of VP, with no light and light. Data expressed as mean \pm SD (n=2).

4 Chapter Conclusion and Future Prospects

In this work, SLN functionalized with DSPE-PEG-FA loaded with VP were proposed as a drug carrier solution to improve the pharmacokinetics and delivery of VP to cancer cells, aiming to enhance its water solubility and selectivity towards tumor cells, limiting systemic toxic effects and maintaining the high PDT efficiency of the free drug. The strategy proposed in this work proved to be successful, demonstrating a high tumor internalization, low dark toxicity and a high anti-tumoral activity upon light irradiation proving the successfulness of the PDT treatment.

SLN were produced using an organic-solvent free, low-cost production method which may facilitate their large-scale production. SLN presented proper size for the delivery into the bloodstream and tumor targeting by exploiting the EPR effect. VP was efficiently encapsulated within the lipidic matrix of the NPs, showing an EE% greater than 95% that remained high for at least 3 months. Moreover, NPs proved to be suitable for intravenous administration, showing no toxicity to human RBCs.

SLN uptake assays conducted in MCF-7 showed that a 3 h incubation was enough to have a high internalization into MCF-7 cells. In addition, SLN were found to have a low dark toxicity (which was proved in both normal L929 cells and tumoral MCF-7 cells). The light irradiation assays proved to be effective. In fact, all of the assays performed showed clear differences between the non-irradiated and light irradiated samples. This shows that the mechanism of action of VP was maintained, and that there was only toxicity upon light irradiation. The cell viability of MCF-7 assessed after 24h exposure to the NPs and 5 min light irradiation revealed their therapeutic efficacy for concentrations as low as 1 μ M of drug. This was also corroborated by an enhanced apoptosis and ROS production upon light irradiation. Additionally, PDT was accomplished using an economic light source (LED source) and low light doses, which may be beneficial in a future clinical application.

The use of nanotechnology in PDT and for VP in particular is of great interest, as it can contribute to an enhanced drug delivery to cancer cells, limited distribution in the normal healthy tissues while improving the drug solubility and bioavailability. The results here highlighted suggest that the developed nanoformulation in combination with the LED light source hold great promise for a future PDT clinical application.

For future prospects it would be interesting to study the different mechanisms of cell entry of the free VP and VP-loaded SLN. It would also be relevant to study other time points of cellular uptake to verify the advantage of the SLN functionalization. A quantitative assay to measure cellular uptake could also be performed using flow cytometry, In addition, PDT studies with other cancer cell lines could also be carried out to ensure the versatility of this therapeutic approach in different cancer types. Additionally, PDT can also be combined with other treatment modalities such as chemotherapy. In this context preliminary studies have been carried out using the drug epirubicin, an antineoplastic, acting specifically during the S phase of cell division, inhibiting DNA and RNA synthesis, used to prevent the appearance of metastases [123]. In the future it would be interesting to have a multimodal treatment combining VP as PS and epirubicin as a chemotherapeutic agent, thus enhancing the efficacy of the treatment and reducing drug dosages.

Finally, studies in healthy and disease animal models could be carried out to evaluate the biodistribution, safety and therapeutic potential of the nanoformulations with and without light irradiation.

Appendix

Preliminary studied aiming to produce lipid nanoparticles for the encapsulation of epirubicin (Figure S1) have been carried out. A calibration curve of the drug in PBS was performed for future quantification studies, including the determination of the EE (Figure S2). After that, various types of nanoformulations loaded with epirubicin have been produced to evaluate which formulation was the most adequate, taking into account parameters such as the size of the nanoparticle, the EE and its stability over time. To do so, different amounts of Cetyl palmitate and Tween 80 were studied. In addition, NLC were also produced by incorporating Mygliol to the nanoformulation. The evaluation of the particle diameters was performed using both DLS and Nanoparticle tracking analysis (NTA). NTA is a system for the determination of particle sizes ranging from 30 to 1000 nm. NTA consists of an analytical method that combines laser light scattering microscopy with a charge-coupled device camera. The NTA program enables the observation and tracking of individual NPs in Brownian motion and connects the motion to a particle size using a calculation based on the Stokes-Einstein equation, providing to be a more accurate evaluation of its real diameter [124].

NPs have been produced with a good EE and diameters below 200 nm (assessed by DLS). Based on these results, the best formulation composition was chosen as follows: 210mg Cetyl palmitate, 70mg Tween 80, 5mg epirubicin, 2mg DSPE-PEG-FA. The produced nanoformulations were further characterized in terms of size, PDI, zeta potential and EE as shown in Table S1. The sizes determined using DLS show slightly higher size than in NTA but still within the suitable range for IV injection. PDI remained at values below 0.2, suggesting that a homogenous population of NPs was obtained, and it was also evident that the size of the NPs was not greatly impacted by the functionalization [117]. Zeta potential was in the range of -11 to 3 mV in the nanoformulations produced, which is value considered neutral, which can be attributed to the ionic strength of the PBS, used as the solvent [125]. Very high values of EE were obtained for both functionalized and non-functionalized SLN, which suggests that the developed SLN are suitable nanocarriers for epirubicin.

Figure S 3 - Molecular structure of epirubicin

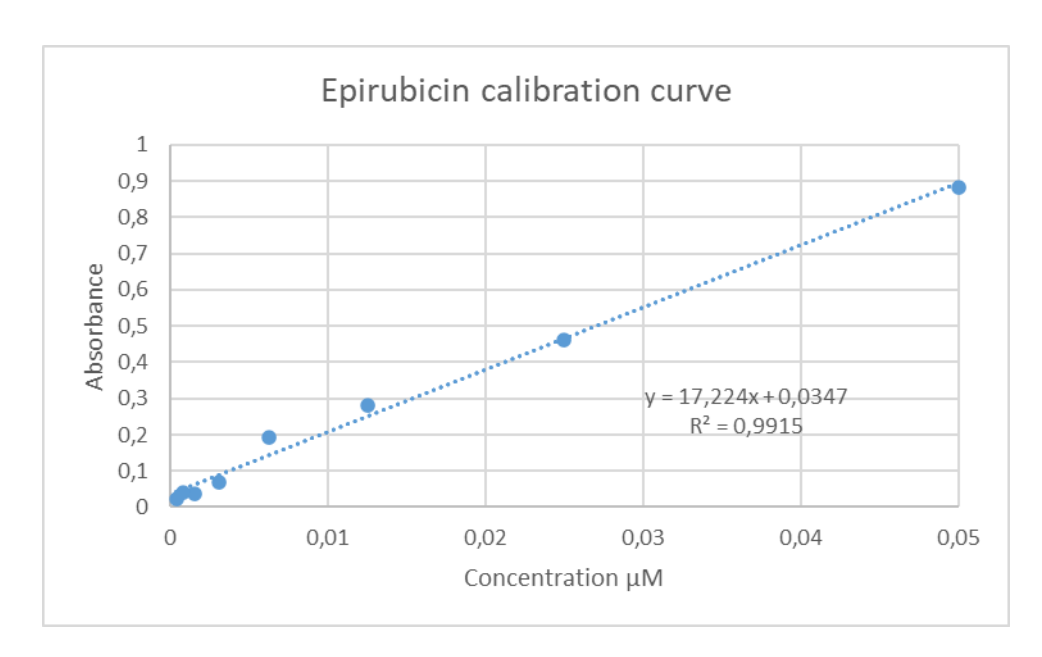


Figure S $_2$ - Calibration curve of epirubicin in PBS pH $_8$ 2. Linear regression was drawn, and the correlation coefficient (R2) calculated. Linearity of the standard curve and a satisfactory R2 value was observed at the range of concentrations from o to $_{0.05}$ mg/mL

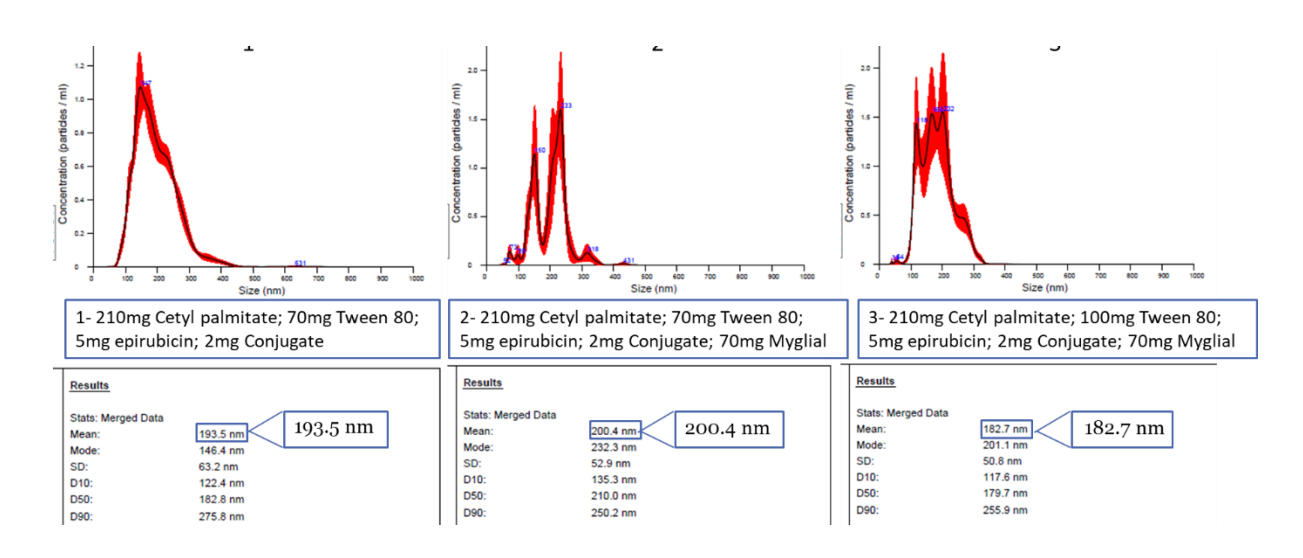


Figure S 1 - NTA analysis of 3 different epirubicin-loaded SLN.

Table S 1 - Physicochemical characterization of the final formulations: size, PDI, zeta potential (obtained using DLS), and EE. Values represent the mean \pm SD (n=3)

	SLN-FA	SLN EPI	SLN-FA-EPI
Size (nm)	233 ± 6	265 ± 2	267 ± 2
PDI	0.16 ± 0.19	0.21 ± 0.01	0.14 ± 0.02
Zeta Potencial (mV)	3 ± 7	-11 ± 6	-7 ± 1
EE (%)	N/A	97 ± 1	96 ± 4

References

- 1. Ruddon, R.W., Cancer biology. 2007, Oxford; New York: Oxford University Press.
- 2. DeVita VT, L.T., Lawrence TS, Rosenberg SA, Devita, Hellman, and Rosenberg's, Cancer: Principles and Practice of Oncology. 11th ed. 2019, Philadelphia.
- 3. Sung, H., et al., Global Cancer Statistics 2020: GLOBOCAN Estimates of Incidence and Mortality Worldwide for 36 Cancers in 185 Countries. CA Cancer J Clin, 2021. 71(3): p. 209-249.
- 4. https://progressreport.cancer.gov/after/economic_burden. August 2022].
- 5. Luengo-Fernandez, R., et al., *Economic burden of cancer across the European Union:* a population-based cost analysis. Lancet Oncol, 2013. 14(12): p. 1165-74.
- 6. Palesh, O., et al., Management of side effects during and post-treatment in breast cancer survivors. The Breast Journal, 2018. 24(2): p. 167-175.
- 7. Numico, G., et al., Cancer survivorship: long-term side-effects of anticancer treatments of gastrointestinal cancer. Current Opinion in Oncology, 2015. 27(4): p. 351-357.
- 8. Tang, W.-L., W.-H. Tang, and S.-D. Li, *Cancer theranostic applications of lipid-based nanoparticles*. Drug Discovery Today, 2018. 23(5): p. 1159-1166.
- 9. Sanchez-Moreno, P., et al., *Smart Drug-Delivery Systems for Cancer Nanotherapy*. Curr Drug Targets, 2018. 19(4): p. 339-359.
- 10. Ediriwickrema, A. and W.M. Saltzman, *Nanotherapy for Cancer: Targeting and Multifunctionality in the Future of Cancer Therapies*. ACS Biomater Sci Eng, 2015. 1(2): p. 64-78.
- 11. Tapeinos, C., M. Battaglini, and G. Ciofani, *Advances in the design of solid lipid nanoparticles and nanostructured lipid carriers for targeting brain diseases*. Journal of Controlled Release, 2017. 264: p. 306-332.
- 12. Raucher, D., S. Dragojevic, and J. Ryu, *Macromolecular Drug Carriers for Targeted Glioblastoma Therapy: Preclinical Studies, Challenges, and Future Perspectives*. Front Oncol, 2018. 8: p. 624.

- 13. Ackroyd, Roger, Clive Kelty, Nicola Brown, and Malcolm Reed. The history of photodetection and photodynamic therapy. Photochemistry and Photobiology, 74, 5 (2001), 656 669.
- 14. Dolmans, D., Fukumura, D., Jain, R. Photodynamic therapy for cancer. Nature Reviews Cancer. 3, 5.
- 15. Daniel, M. D., Hill, J. S. A history of photodynamic therapy. Australian and New Zealand Journal of Surgery. 61, 5.
- 16. Yoon, I., Li, J., Shim, Y. Advance in Photosensitizers and Light Delivery for Photodynamic Therapy. Clinical Endoscopy. 46, 1 (2013), 7 23.
- 17. Castano, A. P., Deminova, T. N., Hamblin, M. R. Mechanisms in photodynamic therapy: Part one Photosensitizers, photochemistry and cellular localization. Photodiagnosis and Photodynamic Therapy. 1, 4 (2004), 279 293.
- 18. Triesscheijn, M., Baas, P., Schellens, J., Stewart, F. (2006). Photodynamic therapy in oncology. The oncologist 11 (9): 1034-44.
- 19. Calzavara-Pinton, P., Venturini, M., Sala, R. Photodynamic therapy: Update 2006
 Part 1: Photochemistry and photobiology. Journal of the European Academy of
 Dermatology and Venereology. 21,3 (2007), 293 302.
- 20. Robertson, C.A., D.H. Evans, and H. Abrahamse, *Photodynamic therapy (PDT): a* short review on cellular mechanisms and cancer research applications for *PDT*. Journal of photochemistry and photobiology. B, Biology, 2009, 96(1): p. 1-8.
- 21. Castano, A.P., P. Mroz, and M.R. Hamblin, *Photodynamic therapy and anti-tumour immunity*. Nat Rev Cancer, 2006. 6(7): p. 535-45.
- 22. Castano, A.P., T.N. Demidova, and M.R. Hamblin, *Mechanisms in photodynamic therapy: part two-cellular signaling, cell metabolism and modes of cell death.* Photodiagnosis Photodyn Ther, 2005. 2(1): p. 1-23.
- 23. Kessel, D.; Oleinick, N.L. Cell Death Pathways Associated with Photodynamic Therapy: An Update. Photochem. Photobiol. 2018, 94, 213–218.
- 24. De Silva, P.; Saad, M.A.; Thomsen, H.C.; Bano, S.; Ashraf, S.; Hasan, T. Photodynamic Therapy, Priming and Optical Imaging: Potential Co-Conspirators in

- Treatment Design and Optimization—A Thomas Dougherty Award for Excellence in PDT Paper. J. Porphyr. Phthalocyanines 2020, 24, 1320–1360.
- 25. Mahalingam, S.M.; Ordaz, J.D.; Low, P.S. Targeting of a Photosensitizer to the Mitochondrion Enhances the Potency of Photodynamic Therapy. ACS Omega 2018, 3, 6066–6074
- 26. Mroz, P., Yaroslavsky, A., Kharkwal, G., Hamblin, M. Cell Death Pathways in Photodynamic Therapy of Cancer. Cancer. 3, 2 (2011). 2516 2539.
- 27. L. Galluzzi, I. Vitale, J.M. Abrams, E.S. Alnemri, E.H. Baehrecke, M.V. Blagosklonny, T.M. Dawson, V.L. Dawson, W.S. El-Deiry, S. Fulda, E. Gottlieb, D.R. Green, M.O. Hengartner, O. Kepp, R.A. Knight, S. Kumar, S.A. Lipton, X. Lu, F. Madeo, W. Malorni, P. Mehlen, G. Nunez, M.E. Peter, M. Piacentini, D.C. Rubinsztein, Y. Shi, H.U. Simon, P. Vandenabeele, E. White, J. Yuan, B. Zhivotovsky, G. Melino, and G. Kroemer. Molecular definitions of cell death subroutines: recommendations of the Nomenclature Committee on Cell Death 2012. Cell death and differentiation, 2012, 19(1), 107-20.
- 28. Song, C.; Xu, W.; Wu, H.; Wang, X.; Gong, Q.; Liu, C.; Liu, J.; Zhou, L. Photodynamic Therapy Induces Autophagy-Mediated Cell Death in Human Colorectal Cancer Cells via Activation of the ROS/JNK Signaling Pathway. Cell Death Dis. 2020, 11.
- 29. Allison, R.R.; Moghissi, K. Photodynamic Therapy (PDT): PDT Mechanisms. Clin. Endosc. 2013, 46, 24–29
- 30. Garg, A.D.; Nowis, D.; Golab, J.; Agostinis, P. Photodynamic Therapy: Illuminating the Road from Cell Death towards AntiTumour Immunity. Apoptosis 2010, 15, 1050–1071.
- 31. Cavaco, A., et al., Collateral Damage Intended—Cancer-Associated Fibroblasts and Vasculature Are Potential Targets in Cancer Therapy. International Journal of Molecular Sciences, 2017. 18(11): p. 2355.
- 32. Sia, J., et al., Molecular Mechanisms of Radiation-Induced Cancer Cell Death: A Primer. Front Cell Dev Biol, 2020. 8: p. 41.
- 33. Khong, H.T.; Restifo, N.P. Natural Selection of Tumor Variants in the Generation of "Tumor Escape" Phenotypes. Nat. Immunol. 2002, 3, 999–1005

- 34. Reginato, E., P. Wolf, and M.R. Hamblin, *Immune response after photodynamic therapy increases anti-cancer and anti-bacterial effects*. World J Immunol, 2014. 4(1): p. 1-11.
- 35. Gollnick, S.O.; Evans, S.S.; Baumann, H.; Owczarczak, B.; Maier, P.; Vaughan, L.; Wang, W.C.; Unger, E.; Henderson, B.W. Role of Cytokines in Photodynamic Therapy-Induced Local and Systemic Inflammation. Br. J. Cancer 2003, 88, 1772–1779
- 36. Cecic, I.; Korbelik, M. Mediators of Peripheral Blood Neutrophilia Induced by Photodynamic Therapy of Solid Tumors. Cancer Lett. 2002, 183, 43–51.
- 37. Krysko, D.V.; Garg, A.D.; Kaczmarek, A.; Krysko, O.; Agostinis, P.; Vandenabeele, P. Immunogenic Cell Death and DAMPs in Cancer Therapy. Nat. Rev. Cancer 2012, 12, 860–875
- 38. Nath, S.; Obaid, G.; Hasan, T. The Course of Immune Stimulation by Photodynamic Therapy: Bridging Fundamentals of Photochemically-Induced Immunogenic Cell Death to the Enrichment of T Cell Repertoire. Photochem. Photobiol. 2019, 95, 1288–1305
- 39. Calixto, G.M.F., et al., Nanotechnology-Based Drug Delivery Systems for Photodynamic Therapy of Cancer: A Review. Molecules, 2016. 21(3): p. 342.
- 40. Rocha, L.G.B. Development of a Novel Photosensitizer for Photodynamic Therapy of Cancer. Ph.D. Thesis, University of Coimbra, Coimbra, Portugal, 2015.
- 41. Lange, N., et al., *Potential of Cyanine Derived Dyes in Photodynamic Therapy*. Pharmaceutics, 2021. 13(6): p. 818.
- 42. Hu Z, Oleinick N, Hamblin MR (2014) Photodynamic Therapy as an Emerging Treatment Modality for Cancer and Non-Cancer Diseases. J Anal Bioanal Tech S1:e001. doi: 10.4172/2155-9872.S1-e001.
- 43. Nowak-Stepniowska, A., P. Pergoł, and A. Padzik-Graczyk, [Photodynamic method of cancer diagnosis and therapy--mechanisms and applications]. Postepy Biochem, 2013. 59(1): p. 53-63.
- 44. J. Kou, D. Dou, L. Yang, Porphyrin photosensitizers in photodynamic therapy and its applications, Oncotarget 8 (2017) 81591–81603

- 45. E.S. Nyman, P.H. Hynninen, Research advances in the use of tetrapyrrolic photosensitizers for photodynamic therapy, J. Photochem. Photobiol. B 73 (2004) 1–28
- 46. Juzeniene, A., Peng, Q., Moan, J., 2007. Milestones in the development of photodynamic therapy and fluorescence diagnosis. Photochemical and photobiological sciences: Official journal of the European Photochemistry Association and the European Society for Photobiology 6 (12): 1234-45.
- 47. Agostinis, P., Berg, K., Cengel, K., Foster, T., Girotti, A., Gollnick, S., Hahn, S., Hamblin, M., Juzeniene, A., Kessel, D., Korbellick, M., Moan, J., Mroz, P., Nowis, D., Piette, J., Wilson. B., Golab, J. (2011). Photodynamic therapy of cancer: An update. CA Cancer journal for clinicians 61: 250-281.
- 48. Nagata, J.Y., et al., *Antibacterial photodynamic therapy for dental caries: evaluation of the photosensitizers used and light source properties.* Photodiagnosis Photodyn Ther, 2012. 9(2): p. 122-31.
- 49. J. Zhang, C. Jiang, J.P. Figueiró Longo, R.B. Azevedo, H. Zhang, L.A. Muehlmann, An updated overview on the development of new photosensitizers for anticancer photodynamic therapy, Acta Pharm. Sin. B 8 (2018) 137–146
- 50. D.K. Chatterjee, L.S. Fong, Y. Zhang, Nanoparticles in photodynamic therapy: an emerging paradigm, Adv. Drug Deliv. Rev. 60 (2008) 1627–1637
- 51. K. Moriwaki, T. Sawada, M. Akiyama, A. Ikeda, J. Kikuchi, T. Matsumura, S. Yano, H. Kataoka, M. Inoue, H. Akashi, Synthesis and photophysical properties of S Mannosylated chlorins and their effect on photocytotoxicity in HeLa cells, Bull. Chem. Soc. Jpn. 91 (2018) 230–236.
- 52. H. Kataoka, H. Nishie, N. Hayashi, M. Tanaka, A. Nomoto, S. Yano, T. Joh, New photodynamic therapy with next-generation photosensitizers, Ann. Transl. Med. 5 (2017) 183.
- 53. M.D. Savellano, T. Hasan, Targeting cells that overexpress the epidermal growth factor receptor with polyethylene glycolated BPD verteporfin photosensitizer immunoconjugates, Photochem. Photobiol. 77 (2003) 431–439.
- 54. Greco, A., et al., *Nanotechnology, a booster for the multitarget drug verteporfin.*Journal of Drug Delivery Science and Technology, 2021. 64.

- 55. Schmidt-Erfurth, U. and T. Hasan, *Mechanisms of Action of Photodynamic Therapy* with Verteporfin for the Treatment of Age-Related Macular Degeneration. Survey of Ophthalmology, 2000. 45(3): p. 195-214.
- 56. K. Tokarska, et al., "Evaluation of nanoencapsulated verteporfin's cytotoxicity using a microfluidic system, J. Pharmaceut. Biomed. Anal. 127 (Aug. 2016) 39–48.
- 57. Weijer, R., et al., Enhancing photodynamic therapy of refractory solid cancers: Combining second-generation photosensitizers with multi-targeted liposomal delivery. Journal of Photochemistry and Photobiology C: Photochemistry Reviews, 2015. 23: p. 103-131.
- 58. A.M. Richter, E. Waterfield, A.K. Jain, A.J. Canaan, B.A. Allison, J.G. Levy, Liposomal delivery of a photosensitizer, benzoporphyrin derivative monoacid ring A (BPD), to tumor tissue in a mouse tumor model, Photochem. Photobiol. 57 (6) (Jun. 1993) 1000–1006.
- 59. C.T. Supuran, Agents for the prevention and treatment of age-related macular degeneration and macular edema: a literature and patent review, Expert Opin. Ther. Pat. 29 (10) (Oct. 2019) 761–767.
- 60. G. Huber, J. Levy, Development of verteporfin therapy: a collaboration between pharmaceutical companies, device manufacturers and clinical investigators, Semin. Ophthalmol. 16 (4) (Dec. 2001) 213–217.
- 61. L. Morizur, H. Elise, M. Christelle, B. M'Barek Karim, Human pluripotent stem cells: a toolbox to understand and treat retinal degeneration, Mol. Cell. Neurosci. (Jul. 2020) 103523.
- 62. S.B. Brown, K.J. Mellish, Verteporfin: a milestone in opthalmology and photodynamic therapy, Expet Opin. Pharmacother. 2 (2) (Feb. 2001) 351–361.
- 63. S.M. Banerjee, et al., Photodynamic therapy in primary breast cancer, J. Clin. Med. 9 (2) (Feb. 2020).
- 64. K. Kaneko, et al., Heat shock protein 90-targeted photodynamic therapy enables treatment of subcutaneous and visceral tumors, Commun. Biol. 3 (1) (May 2020) 226.
- 65. M.T. Huggett, et al., Phase I/II study of verteporfin photodynamic therapy in locally advanced pancreatic cancer, Br. J. Canc. 110 (7) (Apr. 2014) 1698–1704.

- 66. Hong, E.J., D.G. Choi, and M.S. Shim, *Targeted and effective photodynamic therapy* for cancer using functionalized nanomaterials. Acta Pharmaceutica Sinica B, 2016. 6(4): p. 297-307.
- 67. Mokwena, M.G., et al., *A review of nanoparticle photosensitizer drug delivery uptake* systems for photodynamic treatment of lung cancer. Photodiagnosis Photodyn Ther, 2018. 22: p. 147-154.
- 68. Abrahamse, H. and M.R. Hamblin, *New photosensitizers for photodynamic therapy*. Biochem J, 2016. 473(4): p. 347-64.
- 69. Chen, G., et al., Nanochemistry and Nanomedicine for Nanoparticle-based Diagnostics and Therapy. Chem Rev, 2016. 116(5): p. 2826-85.
- Naidoo, C., C.A. Kruger, and H. Abrahamse, *Photodynamic Therapy for Metastatic Melanoma Treatment: A Review*. Technology in Cancer Research & Treatment, 2018.
 17: p. 1533033818791795.
- 71. Shah, S.R., et al., Verteporfin-Loaded Polymeric Microparticles for Intratumoral Treatment of Brain Cancer. Molecular Pharmaceutics, 2019. 16(4): p. 1433-1443.
- 72. Zhou, Y., X. Liang, and Z. Dai, *Porphyrin-loaded nanoparticles for cancer theranostics*. Nanoscale, 2016. 8(25): p. 12394-12405.
- 73. Moghassemi, S., et al., *Photodynamic cancer therapy using liposomes as an advanced vesicular photosensitizer delivery system.* Journal of Controlled Release, 2021. 339: p. 75-90.
- 74. Czarnecka-Czapczynska, M., et al., *The role of photodynamic therapy in breast cancer A review of in vitro research*. Biomed Pharmacother, 2021. 144: p. 112342.
- 75. G. Obaid, M. Broekgaarden, A.L. Bulin, H.C. Huang, J. Kuriakose, J. Liu, T. Hasan, Photonanomedicine: a convergence of photodynamic therapy and nanotechnology, Nanoscale 8 (2016) 12471–12503.
- 76. Olivo, M., et al., Targeted Therapy of Cancer Using Photodynamic Therapy in Combination with Multi-faceted Anti-Tumor Modalities. Pharmaceuticals, 2010. 3(5): p. 1507-1529.
- 77. Lim, C.-K., et al., Nanophotosensitizers toward advanced photodynamic therapy of Cancer. Cancer Letters, 2013. 334(2): p. 176-187.

- 78. Deng, K., et al., Recent Progress in Near Infrared Light Triggered Photodynamic Therapy. Small, 2017. 13(44).
- 79. Debele, T.A., S. Peng, and H.C. Tsai, *Drug Carrier for Photodynamic Cancer Therapy*. Int J Mol Sci, 2015. 16(9): p. 22094-136.
- 80. Mahesh, G.A.; Vijayalakshmi, A.; Madhusudhana, R.N.; Manorama, V.S. Chlorin e6 loaded lactoferrin nanoparticles for enhanced photodynamic therapy. J. Mater. Chem. B 2018, 5, 9189–9196.
- 81. Montaseri, H., C.A. Kruger, and H. Abrahamse, *Review: Organic nanoparticle based active targeting for photodynamic therapy treatment of breast cancer cells.*Oncotarget, 2020. 11(22): p. 2120-2136.
- 82. Pearce, A.K. and R.K. O'Reilly, *Insights into Active Targeting of Nanoparticles in Drug Delivery: Advances in Clinical Studies and Design Considerations for Cancer Nanomedicine*. Bioconjugate Chemistry, 2019. 30(9): p. 2300-2311.
- 83. Mehnert, W. and K. Mäder, *Solid lipid nanoparticles: production, characterization and applications*. Adv Drug Deliv Rev, 2001. 47(2-3): p. 165-96.
- 84. Ameya Deshpande, M.M., Saloni B. Daftardar, Meghavi Patel, Sai H.S. Boddu, Jerry Nesamony, Chapter 12. Solid Lipid Nanoparticles in Drug Delivery: Opportunities and Challenges, in Emerging Nanotechnologies for Diagnostics, Drug Delivery and Medical Devices, A.M.K.C.A. Mandal, Editor. 2017, Elsevier. p. 291-330.
- 85. Shah, R.M., et al., Transport of stearic acid-based solid lipid nanoparticles (SLNs) into human epithelial cells. Colloids Surf B Biointerfaces, 2016. 140: p. 204-212.
- 86. Ghasemiyeh, P. and S. Mohammadi-Samani, Solid lipid nanoparticles and nanostructured lipid carriers as novel drug delivery systems: applications, advantages and disadvantages. Res Pharm Sci, 2018. 13(4): p. 288-303.
- 87. Pardeike, J., A. Hommoss, and R.H. Müller, Lipid nanoparticles (SLN, NLC) in cosmetic and pharmaceutical dermal products. Int J Pharm, 2009. 366(1-2): p. 170-84.
- 88. Borges, A., et al., Solid Lipid Nanoparticles as Carriers of Natural Phenolic Compounds. Antioxidants (Basel), 2020. 9(10).

- 89. Rajabi, M. and S.A. Mousa, *Lipid Nanoparticles and their Application in Nanomedicine*. Curr Pharm Biotechnol, 2016. 17(8): p. 662-72.
- 90. Naseri, N., Valizadeh, H., Zakeri-Milani, P., 2015. Solid lipid nanoparticles and nanostructured lipid carriers: structure, preparation and application. Adv. Pharm. Bull. 5 (3).
- 91. Shah, R., D. Eldridge, E. Palombo, and I. Harding, Lipid nanoparticles: Production, characterization and stability. 2015: Springer.
- 92. Poovi Ganesan, D.N., Lipid nanoparticles: Different preparation techniques, characterization, hurdles, and strategies for the production of solid lipid nanoparticles and nanostructured lipid carriers for oral drug delivery. Sustainable Chemistry and Pharmacy, 2017. 6: p. 37-56.
- 93. Müller, R.H., K. Mäder, and S. Gohla, *Solid lipid nanoparticles (SLN) for controlled drug delivery a review of the state of the art*. Eur J Pharm Biopharm, 2000. 50(1): p. 161-77.
- 94. Fernández, M., F. Javaid, and V. Chudasama, *Advances in targeting the folate receptor in the treatment/imaging of cancers*. Chem Sci, 2018. 9(4): p. 790-810.
- 95. Granja, A., et al., *Mitoxantrone-loaded lipid nanoparticles for breast cancer therapy* Quality-by-design approach and efficacy assessment in 2D and 3D in vitro cancer models. Int J Pharm, 2021. 607: p. 121044.
- 96. PubChem Compound Summary for CID 10889, Cetyl palmitate. . 2021 September 13, 2021].
- 97. Garidel, P., C. Hoffmann, and A. Blume, A thermodynamic analysis of the binding interaction between polysorbate 20 and 80 with human serum albumins and immunoglobulins: a contribution to understand colloidal protein stabilisation. Biophys Chem, 2009. 143(1-2): p. 70-8.
- 98. van Steenis, J.H., E.M. van Maarseveen, F.J. Verbaan, R. Verrijk, D.J. Crommelin, G. Storm, and W.E. Hennink, Preparation and characterization of folate-targeted pEG-coated pDMAEMA-based polyplexes. J Control Release, 2003. 87(1-3): p. 167-76.
- 99. Chan, P., M. Kurisawa, J.E. Chung, and Y.Y. Yang, Synthesis and characterization of chitosan-g-poly(ethylene glycol)-folate as a non-viral carrier for tumor-targeted gene delivery. Biomaterials, 2007. 28(3): p. 540-549.

- 100. Satinder K.Brar, M.V., *Measurement of nanoparticles by light-scattering techniques*. TrAC Trends in Analytical Chemistry, 2011. 30(1): p. 4-17.
- 101. Lin, P.C., et al., *Techniques for physicochemical characterization of nanomaterials*. Biotechnol Adv, 2014. 32(4): p. 711-26.
- 102. Kumar, N.a.S.K., *Essentials in Nanoscience and Nanotechnology*. 2016: John Wiley & Son.
- 103. Zeta Potential Measurements. 13 september 2021]; Available from: https://www.microtrac.com/products/zeta-potential/.
- 104. Gumustas, M., et al., Chapter 5 Effect of Polymer-Based Nanoparticles on the Assay of Antimicrobial Drug Delivery Systems, in Multifunctional Systems for Combined Delivery, Biosensing and Diagnostics, A.M. Grumezescu, Editor. 2017, Elsevier. p. 67-108.
- 105. Chang, T.M.S., Selected topics in nanomedicine. Vol. 3. 2013: World Scientific.
- 106. Greco, I., et al., *Correlation between hemolytic activity, cytotoxicity and systemic in vivo toxicity of synthetic antimicrobial peptides.* Sci Rep, 2020. 10(1): p. 13206.
- 107. Guo, Q., et al., Functional silver nanocomposites as broad-spectrum antimicrobial and biofilm-disrupting agents. ACS Appl. Mater. Interfaces, 2017. 9(20): p. 16834-47.
- 108. Pipintakos, G., et al., Application of Atomic Force (AFM), Environmental Scanning Electron (ESEM) and Confocal Laser Scanning Microscopy (CLSM) in bitumen: A review of the ageing effect. Micron, 2021. 147: p. 103083.
- 109. Nakayama, G.R., et al., *Assessment of the Alamar Blue assay for cellular growth and viability in vitro*. J Immunol Methods, 1997. 204(2): p. 205-8.
- 110. O'Brien, J., et al., *Investigation of the Alamar Blue (resazurin) fluorescent dye for the assessment of mammalian cell cytotoxicity*. Eur J Biochem, 2000. 267(17): p. 5421-6.
- 111. Alfonso, B.F. and M. Al-Rubeai, 1.42 Flow Cytometry, in Comprehensive Biotechnology (Second Edition), M. Moo-Young, Editor. 2011, Academic Press: Burlington. p. 559-578.

- 112. Figueroa, D., M. Asaduzzaman, and F. Young, Real time monitoring and quantification of reactive oxygen species in breast cancer cell line MCF-7 by 2',7'—dichlorofluorescin diacetate (DCFDA) assay. Journal of Pharmacological and Toxicological Methods, 2018. 94: p. 26-33.
- 113. Mihaljevic, O., et al., *Apoptosis and genome instability in children with autoimmune diseases*. Mutagenesis, 2018. 33(5-6): p. 351-357.
- 114. Attia, M.F., et al., An overview of active and passive targeting strategies to improve the nanocarriers efficiency to tumour sites. J Pharm Pharmacol, 2019. 71(8): p. 1185-1198.
- 115. Huang, D., et al., Nanodrug Delivery Systems Modulate Tumor Vessels to Increase the Enhanced Permeability and Retention Effect. J Pers Med, 2021. 11(2).
- 116. Singh, R. and J.W. Lillard, Jr., *Nanoparticle-based targeted drug delivery*. Exp Mol Pathol, 2009. 86(3): p. 215-23.
- 117. Danaei, M., et al., Impact of Particle Size and Polydispersity Index on the Clinical Applications of Lipidic Nanocarrier Systems. Pharmaceutics, 2018. 10(2).
- 118. Mehmet Gumustas, C.T.S.-T., Aysen Gumustas, Sibel A. Ozkan, Bengi Uslu, *Effect of Polymer-Based Nanoparticles on the Assay of Antimicrobial Drug Delivery Systems*, in *Multifunctional Systems for Combined Delivery, Biosensing and Diagnostics*, A.M. Grumezescu, Editor. 2017. p. 67-108.
- 119. Standard, I., ISO 10993-4: Biological Evaluation of Medical Devices Part 4—Selection of Tests for Interactions with Blood. 2017, International Organization for Standardization: Geneva, Switzerland.
- 120. Chen, Y.A., et al., Effect of Cerenkov Radiation-Induced Photodynamic Therapy with (18)F-FDG in an Intraperitoneal Xenograft Mouse Model of Ovarian Cancer. Int J Mol Sci, 2021. 22(9).
- 121. Standardization, I. O. F Biological Evaluation of Medical Devices—Part 5: Tests for in Vitro Cytotoxicity; International Standard ISO 10993-5: Geneva, Switzerland, 2009.
- 122. Wei, H., et al., Verteporfin suppresses cell survival, angiogenesis and vasculogenic mimicry of pancreatic ductal adenocarcinoma via disrupting the YAP-TEAD complex. Cancer Sci, 2017. 108(3): p. 478-487.

- 123. Wang, X.F., et al., *Epirubicin inhibits growth and alters the malignant phenotype of the U-87 glioma cell line*. Mol Med Rep, 2015. 12(4): p. 5917-5923.
- 124. Filipe, V., A. Hawe, and W. Jiskoot, *Critical evaluation of Nanoparticle Tracking Analysis (NTA) by NanoSight for the measurement of nanoparticles and protein aggregates.* Pharm Res, 2010. 27(5): p. 796-810.
- 125. Clogston, J.D. and A.K. Patri, *Zeta potential measurement*. Methods Mol Biol, 2011. 697: p. 63-70.